REMARKS

Claims 1-30 and 54 are pending in the application, and are subject to restriction. Independent claims 1, 20, and 54 have been revised to recite a solid oxide fuel cell that is prepared by a process whereby at least the solid electrolyte and anode being prepared by co-firing or sintering at least two layers to form a porous anode layer and a dense solid electrolyte layer, and then impregnating the porous anode layer with an aqueous solution containing a salt of at least ceria. Support for the amendments can be found throughout the specification and examples, and specifically at page 12, lines 16 and 17 for claim 54, ("aqueous impregnation using a concentrated salt solution), and page 13, lines 6 and 7 for claims 1 and 20 ("[o]ther components including ceria oxide (CeO_2), are preferably added using the same impregnation methods. No new matter is presented by the amendments, the amendments simplify issues for appeal, and the amendments place the claims in condition for allowance. Accordingly, applicants respectfully request entry thereof and reconsideration of claims 1-30 and 54 in light of the following remarks.

Initially, applicants wish to thank Examiner Yuan for the courtesies extended the undersigned during the telephonic interview on January 21, 2005. Applicants' representative discussed the amendments now made to the claims, and the prior art, including a new document that has not yet been cited, but that has been cited in corresponding foreign applications. No agreement was reached, although the Examiner encouraged applicants to file the amendments presented herewith.

Turning now to the Action, claim 54 is alleged to be directed to an invention that is independent or distinct from the invention originally claimed. Specifically, the Action alleges that "a solid oxide fuel cell comprising a solid electrolyte. . . a ceramic-metal composite anode containing at least copper and a cathode, . . . is a distinct species from a solid oxide fuel cell comprising a solid electrolyte . . . a ceramic-metal composite anode containing at least copper and a cathode ***as recited in the original claims***." (Action, at page 1, emphasis added). Applicants respectfully disagree with this allegation.

The originally presented claims that have been examined on the merits did not recite any species — copper or ceria. Rather, the claims that were originally presented and examined only recited a solid oxide fuel cell comprising a solid electrolyte comprised of an electronic insulator that allows transfer of anions, a ceramic-metal composite anode and a cathode. It was not until claim 54 was added that the species "ceria" was added to claims 1

and 20. Accordingly, a genus claim covering all of the species now recited in independent claims 1, 20, and 54 has already been examined. Applicants respectfully request that the Examiner reconsider and withdraw the restriction requirement.

Applicants appreciate with thanks the Examiner's withdrawal of the previous rejections under 35 U.S.C. §112, second paragraph.

On pages 2-6 of the Action, claims 1-6, 9-27, and 30 are rejected under 35 U.S.C. §103(a) as being unpatentable over Wallin, U.S. Patent No. 6,017,647 ("Wallin") in view of Anumakonda *et al.*, U.S. Patent No. 6,221,280 ("Anumakonda"). The present Action repeats the previous rejection. For the reasons set forth in applicants' responses filed on September 17, 2003, and August 11, 2004, this rejection is respectfully traversed.

Even assuming that Anumakonda suggests directing a sulfur-containing fuel to a solid oxide fuel cell, Anumakonda clearly states that the fuel cell must be "sulfur tolerant," or alternatively, have a provision for desulfurizing the product gas stream. *See*, col. 11, lines 58-63 of Anumakonda. The fuel cell of Wallin is not "sulfur tolerant," nor does Wallin include a provision for desulfurizing the product gas stream. Rather, Wallin's fuel cell is made from a conventional anode material, nickel (*see*, all of the examples). Applicants attach as an Appendix a series of publications that describe, *inter alia*, the poisoning effect of sulfur-containing impurities on an SOFC anode containing nickel or other conventional anode metals.

All of the solid oxide fuel cells prepared in Wallin's examples include an anode made from nickel — the examples are the only place in Wallin where preparation of an anode is described, since the remaining disclosure of Wallin pertains to the oxygen electrode, or cathode. The publications attached hereto reveal that it was known in the art at the time the present invention was made that sulfur-containing fuels poisoned or otherwise destroyed a fuel cell's operability when the fuel cell anode comprised nickel. Thus, combining Anumakonda with Wallin would have essentially destroyed the viability of Wallin's fuel cell. A person skilled in the art therefore would not have been motivated to combine Anumakonda and Wallin in the manner asserted in the Action.

Applicants traverse this rejection for the following additional reasons. Wallin discloses a composite oxygen electrode/electrolyte structure that contains a variety of materials. The oxygen electrode is the cathode. All of the examples of Wallin that

specifically disclose an anode material utilize nickel, and prepare the anode in a manner similar to the manner disclosed in some of the publications attached hereto. Applicants appreciate the one passing reference in Wallin (as graciously pointed out to applicants' representative by the Examiner during the interview) that the electrode/electrolyte can be the anode or cathode (col. 5, lines 33-36). Applicants respectfully submit that this sentence would not have suggested to the skilled artisan that modifying the anode of Wallin's examples to include cathode materials could somehow render Wallin's solid oxide fuel cell sulfur tolerant. Indeed, this one sentence in Wallin might possibly suggest, at best, that a nickel-containing anode, and an anode comprised of one of the oxygen electrode/electrolyte materials disclosed therein, would provide substantially equivalent results (*i.e.*, they are interchangeable). The present inventors discovered that this was not the case.

The present inventors discovered that anodes containing at least copper and/or ceria are capable of directly processing sulfur-containing fuels. The inventors discovered a method of incorporating relatively low melting materials (like copper) in an anode by initially co-firing the anode layer and the electrolyte layer, impregnating the resulting anode layer with a solution containing a salt of the anode material, and then heating the impregnated anode to drive off the liquid. Conventional methods of preparing anodes containing nickel (nickel cermet was combined with YSZ and co-fired together with the electrolyte layer at temperatures at or about 1250°C as disclosed in Wallin) were not suitable for preparing an anode containing copper since the copper would melt and diffuse out of the ceramic material during sintering. The inventors discovered that that anode needed to be sintered first, and then impregnated with a solution containing a salt of the anode material (e.g., Cu or CeO_2). It was by this method that the inventors were able to prepare a solid oxide fuel cell capable of directly oxidizing sulfur-containing fuels.

Neither Anumakonda nor Wallin disclose making an anode in the manner recited in the claims. Wallin does disclose infiltrating the sintered fuel cell with an aqueous solution containing an electrocatalyst (*see*, paragraph bridging columns 5 and 6 and the examples); none of the electrocatatlyst materials contain ceria or copper.[1] The method of making the solid oxide fuel cell recited in the present claims therefore produces a novel and unobvious solid oxide fuel cell capable of directly oxidizing sulfur-containing hydrocarbons. The

[1] Applicants do note that the paragraph bridging columns 3 and 4 disclose a laundry list of suitable "electronically-conductive materials" and "electrocatalysts," none of these materials includes ceria or copper.

combination of Anumakonda and Wallin fail to suggest the method, and fail to suggest the so[illegible] prepared sulfur tolerant solid oxide fuel cell. Accordingly, applicants respectfully request that the Examiner reconsider and withdraw this rejection.

On pages 6-9 of the Action, claims 1, 2, 7, 8, 20, 28 and 29 are rejected under 35 U.S.C. §103(a) as being unpatentable over Wallin in view of Fasano, *et al.*, U.S. Patent No. 6,051,330 ("Fasano"). The Action repeats the previous rejection. For the reasons set forth in applicants' response filed on September 17, 2003, and August 11, 2004, this rejection is respectfully traversed.

The Action apparently takes the position that the alcohol feeds disclosed in Fasano inherently have sulfur contents of from about 1 ppm to about 5000 ppm. The Examiner correctly notes the legal requirements to establish inherency insofar as the missing feature must necessarily be present in the prior art. The Action also states, however, that "both Fasano et al. and the present application utilize similar alcohols" (page 7 of the Action). The Action states further that "[t]he instant disclosure provides no further description with respect to the nature and characteristic of the alcohols used" (Action, at page 10). These are not accurate statements.

While it certainly is true that the present specification lists some of the same alcohols by name that are listed in Fasano, the present specification also makes clear that the alcohols disclosed and claimed therein contain at least 1 ppm sulfur. This is a very important difference between the alcohols recited in the present claims and the alcohols broadly disclosed in Fasano. As stated in previous responses, and shown by reference to a number of publications, the sulfur content of commercially available methanol for use in fuel cells is typically zero, and at most about 0.5 ppm. Absent any disclosure to the contrary, a person skilled in the art would recognize that the methanol disclosed in Fasano is precisely the type of methanol typically used in fuel cells — that is, methanol with no sulfur.

In sharp contrast to the Fasano disclosure, the alcohols described and claimed in the present specification require sulfur. That is, the present specification contains disclosure that is contrary to conventional wisdom with respect to fuel cells, which is that the alcohols and other fuels contain sulfur. To the extent that commercially available hydrocarbon fuels (such as an alcohol as recited in the dependent claims) contain no sulfur, sulfur can be added. The Examiner will note that sulfur is added to conventional decane in the examples to provide a

sulfur-containing fuel (thiophene was added to hydrocarbons to provide a sulfur-containing hydrocarbon). Accordingly, the combination of Fasano and Wallin would not result in a fuel cell containing a fuel comprising a sulfur-containing hydrocarbon, as recited in the present claims.

The combination of Fasano and Wallin also fails to suggest a fuel cell comprised of an anode containing at least ceria and/or copper, or the method of making the solid oxide fuel cell. Both Wallin and Fasano disclose conventional solid oxide fuel cell fabrication techniques (Wallin is discussed above, and Fasano, at col. 6, lines 7-33). The combination of Wallin and Fasano therefore would not result in the presently claimed solid oxide fuel cell. Applicants respectfully request that the Examiner reconsider and withdraw this rejection.

Applicants wish to bring to the Examiner's attention Cable, *et al.*, U.S. Patent No. 5,589,285 ("Cable"). Cable has been cited against claims similar to the originally presented claims (not the currently amended claims) in corresponding foreign applications. Cable was cited in applicants' Information Disclosure Statement dated June 3, 2003, and has been initialed by the Examiner. Accordingly, Cable is of record in the present application.

Cable appears to disclose sulfur tolerant fuel cells. The amended claims recite forming the electrolyte and anode by co-firing the two layers together, which is described in Cable as a "bonded" fuel cell. Cable teaches that bonded fuel cells could not process sulfur, and its disclosure therefore is directed to non-bonded fuel cells with various separator and microslip layers positioned between the electrolyte and electrodes. The present inventors therefore achieved what Cable said was not possible — a bonded sulfur-tolerant fuel cell.

In view of the foregoing, applicants respectfully submit that the present claims are in condition for allowance. An early notice to this effect is earnestly solicited. Should there be any questions concerning this response, Examiner Yuan is invited to contact the undersigned at the telephone number listed below.

Respectfully submitted,

2/2/05
Date

Patrick A. Doody
Reg. No. 35,022

HUNTON & WILLIAMS
1900 K. St., NW
Washington, D.C. 2006-1109
(703) 714-7645

Thermodynamics of sulfur chemisorption on metals. III. Iron and cobalt[a)]

Jon G. McCarty and Henry Wise

Solid State Catalysis Laboratory, SRI International, Menlo Park, California 94025
(Received 2 February 1981; accepted 29 September 1981)

Isosteric heats of chemisorption of sulfur on iron and cobalt have been evaluated from measurements of the equilibrium ratio of H_2S/H_2 gas mixtures in contact with the powdered metals over a temperature range from 677 to 855 K. At low surface coverage of sulfur on cobalt, the heat of chemisorption with respect to 1/2 S_2(g) is -236 ± 15 kJ mol^{-1}. With increasing coverage it decreases to -200 ± 10 kJ mol^{-1}. The heat of sulfur chemisorption on iron is -197 ± 15 kJ mol^{-1}. For equivalent coverage, the thermodynamic activity of sulfur chemisorbed on cobalt exceeds that of iron by approximately one order of magnitude. At low surface coverage (<0.5 saturation coverage), the bond strength of sulfur on the various metals is found to vary in the order: Ni > Co > Ru > Fe.

INTRODUCTION

Sulfur dissolved in metallic iron has a very large free energy potential for segregation to the surface. Preferential surface or grain boundary segregation of small quantities of dissolved sulfur can have profound effects on the mechanical and corrosive properties of iron and its alloys.[1] Poisoning by trace concentrations of gaseous sulfur compounds can alter selectivity and severely limit the lifetime of iron-based catalysts used in such important reactions as the Fischer–Tropsch synthesis[2] and ammonia synthesis.[3] Likewise cobalt and iron–cobalt alloys are susceptible to deleterious catalyst poisoning. The purpose of the present work is to examine the thermodynamics of sulfur chemisorption on iron and cobalt as part of a series of equilibrium sulfur chemisorption studies on various metal surfaces. Previous measurements have dealt with nickel[4] and ruthenium.[5]

Indirectly the thermodynamics of reversible sulfur chemisorption on polycrystalline iron at 1123 K were evaluated by Grabke *et al.*[6–8] by measuring the changes in the initial rates of nitrogenation (with N_2) and carburization (with CH_4) following equilibrium exposure to H_2S–H_2 gas mixtures. Paulitschke *et al.*[7–9] estimated the heat of formation of adsorbed sulfur from segregation studies on iron foils at 973 to 1373 K, using Auger electron spectroscopy to measure the sulfur surface coverage in equilibrium with dissolved sulfur in the bulk. Agrawal *et al.*[10] have shown that the cobalt-catalyzed methanation reaction is almost completely poisoned by as little as 15 ppb H_2S in H_2 at 663 K. It is obvious that the surface coverage with sulfur approaches saturation at sulfur chemical potentials well below those required to produce the bulk sulfides of iron and cobalt.

EXPERIMENTAL

The iron and cobalt samples used in this study were prepared by precipitation of 0.5 M aqueous solutions of ferric or cobaltous nitrate with 60% excess potassium carbonate at 298 K. The precipitates were washed thoroughly with distilled water, dried to 373 K, reduced stepwise in a hydrogen stream at 0.1 MPa for periods of 2 h each at 423, 573, and 723 K, and subsequently cooled to 298 K in helium. The specific surface areas of the two powders were measured by CO adsorption at 298 K following reduction in hydrogen at 773 K for 2 h. For iron the saturation coverage was found to correspond to 20.7 μmol CO/g, and for Co, 24.9 μmol CO/g. The specific surface areas were calculated to be 1.17 m^2/g of Fe and 1.40 m^2/g of cobalt, assuming 1.1×10^{15} CO atoms adsorbed per cm^2 of metal surface area.

The experimental techniques used in this study have been described previously.[4,5] Briefly, we place a sample of the metallic powder ($\sim 5 \times 10^{-3}$ g) on the quartz fritted disk of a microreactor. The microreactor is part of a quartz/Teflon closed loop through which hydrogen recirculates. Sampling valves are used to inject aliquots of a dilute H_2S in H_2 mixture of known composition into the loop and to take samples of the recirculating gas for analysis of the H_2S/H_2 ratio. For H_2S analysis a gas chromatograph is used with a very sensitive photoionization detector, so that H_2S concentrations below 1 ppb in H_2 can be detected. After uniform sulfur adsorption coverage is established, isosteres are determined by varying the reactor temperature and measuring the changes in the H_2S/H_2 ratio of the recirculating gas. Because the amount of sulfur adsorbed is several orders of magnitude greater than the amount of H_2S in the recirculating gas, transfer of sulfur from the surface to the gas phase is sufficiently small during the measurements to have an insignificant effect on surface coverage.

RESULTS

Iron

Isosteres for sulfur chemisorption on iron were determined from the measured thermodynamic chemical potential of gaseous sulfur (as H_2S in H_2 at a total pressure of 1 atm) for several values of sulfur coverage (Fig. 1). The enthalpy and entropy for reversible sulfur adsorption [S(a)]

$$H_2S(g) \rightleftharpoons S(a) + H_2(g) ,$$

[a]Support of the Office of Basic Energy Sciences, Division of Chemical Sciences of the U. S. Department of Energy is gratefully acknowledged.

 0021-9606/82/021162-06$02.10

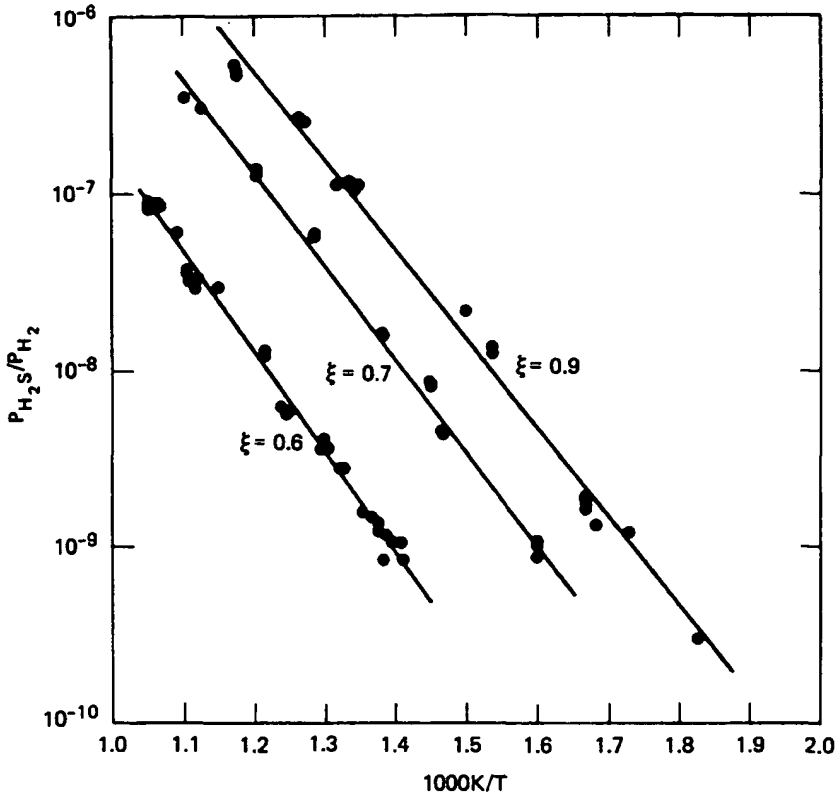

FIG. 1. Sulfur chemisorption isosteres on iron powder.

were calculated from a Van't Hoff analysis of the isosteric data (Table I). Standard enthalpies and entropies of formation for adsorbed sulfur [S(a)] (Table II) were evaluated from the isosteric adsorption data and the tabulated thermodynamic properties of H_2S and H_2 with $S_2(g)$ as the reference state[11] using the relationships

$$\Delta H_f^\circ(T)[S(a)] = \Delta H_{ads}(T) + \Delta H_f^\circ(T)[H_2S(g)] ,$$

and

$$S_f^\circ(T)[S(a)] = \Delta S_{ads}(T) + S_f^\circ(T)[H_2S(g)] - S_f^\circ(T)[H_2(g)] - \tfrac{1}{2}S_f^\circ(T)[S_2(g)] ,$$

where $\Delta H_f^\circ(T)$ and $S_f^\circ(T)$ represent the standard enthalpy and entropy of formation at temperature T. The mean experimental temperature of each isostere was chosen as the reference temperature in the calculations. The normalized sulfur coverage ξ represents the amount of sulfur introduced into the system divided by the CO adsorption capacity at 298 K of the iron powder.

The enthalpies and entropies of sulfur adsorbed on iron are qualitatively similar to those observed previously for nickel[4] and ruthenium.[5] First, the sulfur adspecies are atomic sulfur since adsorption as HS(a) or H_2S(a) would be associated with a much larger entropy of formation. Second, the enthalpy decreases substantially with increasing sulfur coverage.

Cobalt

The chemisorption isosteres of sulfur on cobalt (Fig. 2) were obtained at considerably lower surface coverages -normalized to the CO adsorption capacity of the

TABLE I. Analysis of isosteres for sulfur chemisorption on iron and cobalt.

Metal	Coverage (ξ)[a]	ΔH_{ads}(kJ mol^{-1})	ΔS_{ads}(J mol^{-1} K^{-1})	T_{avg}(K)	n[b]	r[c]
Iron	0.6	−107.8 ± 9.2	21.9 ± 11.1	826	37	0.996
	0.7	−100.7 ± 8.8	10.9 ± 12.2	725	21	0.996
	0.9	− 96.5 ± 10.4	4.9 ± 15.4	677	22	0.994
Cobalt	0.09	−145.1 ± 18.4	2.9 ± 21.5	855	36	0.992
	0.18	−143.4 ± 9.4	− 0.4 ± 11.1	845	14	0.998
	0.3	−150.8 ± 8.3	−14.5 ± 10.0	828	15	0.998
	0.4	−126.7 ± 7.4	9.2 ± 8.8	844	4	0.998
	1.0	−110.2 ± 4.4	−13.3 ± 6.2	702	9	0.999

[a] ξ = coverage normalized to CO uptake at 298 K.
[b] n = number of data points in isostere.
[c] r = least-squares correlation coefficient.

TABLE II. Isosteric heat and entropy of formation of sulfur chemisorbed on iron and cobalt[b]

Metal	Coverage (ξ)[a]	ΔH°_f(kJ mol^{-1})	S°_f(J mol^{-1} K^{-1})	Temperature range (K)
Iron	0.6	−197	105	954–711
	0.7	−189	95	911–625
	0.9	−185	86	855–547
Cobalt	0.09	−234	87	901–803
	0.18	−233	84	898–796
	0.3	−240	69	903–766
	0.4	−216	93	901–794
	1.0	−199	68	752–611

[a]ξ = sulfur coverage normalized to CO uptake at 298 K.
[b]Reference state = $\frac{1}{2}S_2(g)$.

sample). The enthalpy of sulfur adsorption on cobalt is found to be greater than on iron (Table I). Again the standard entropy of adsorption for low surface coverage (Table II) suggests S(a) as the adspecies rather than HS(a) or H_2S(a). At low surface coverage the magnitude of the standard enthalpy of formation of chemisorbed sulfur is approximately 38 kJ mol^{-1} greater for cobalt than for iron. However, as the sulfur coverage increases, ΔH°_f for chemisorption on iron and cobalt (Fig. 3) approaches the values for $\frac{1}{8}$ Co_9S_8 and FeS, respectively. Also the enthalpy difference between chemisorbed sulfur on Fe and Co approaches the difference for the respective bulk sulfides.[12,13]

DISCUSSION

In comparing our results with published thermodynamic values we find that our heat of formation of chemisorbed sulfur on iron at low surface coverage ($\Delta H^\circ_f[S_a]$ = −197 kJ mol^{-1}, Table I) is very close to that calculated from the sum of the heat of segregation[9] (−165 kJ mol^{-1}) and dissolution[14] (−31 kJ mol^{-1}) for polycrystalline iron. Assuming that the saturation coverage of sulfur equals the uptake of carbon monoxide, we find by extrapolation of our data that the equilibrium sulfur activity in the gas (H_2S/H_2) for one-half saturation coverage at 1123 K corresponds to 0.7 ppm. From the data by Grabke *et al.*[8] one obtains a sulfur activity of 0.8 ppm (H_2S/H_2) for this degree of surface coverage at 1123 K. The agreement is most satisfactory considering the different experimen-

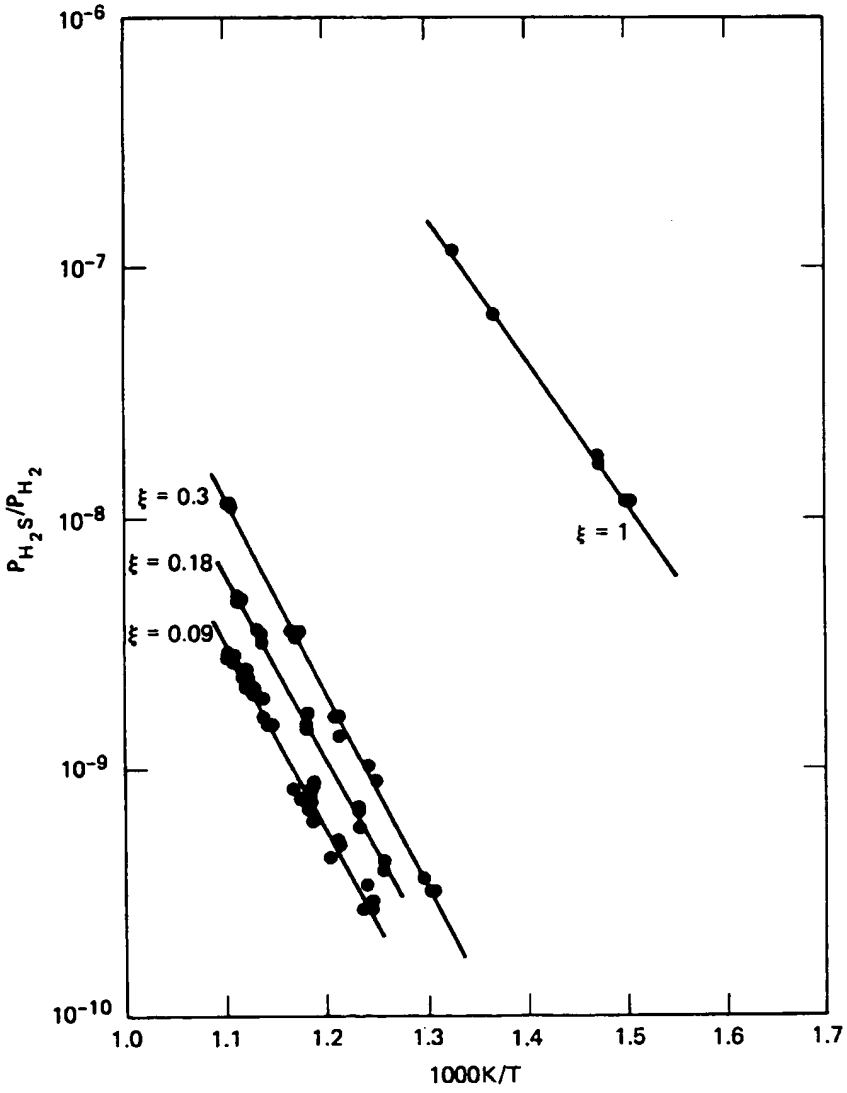

FIG. 2. Sulfur chemisorption isosteres on powdered cobalt.

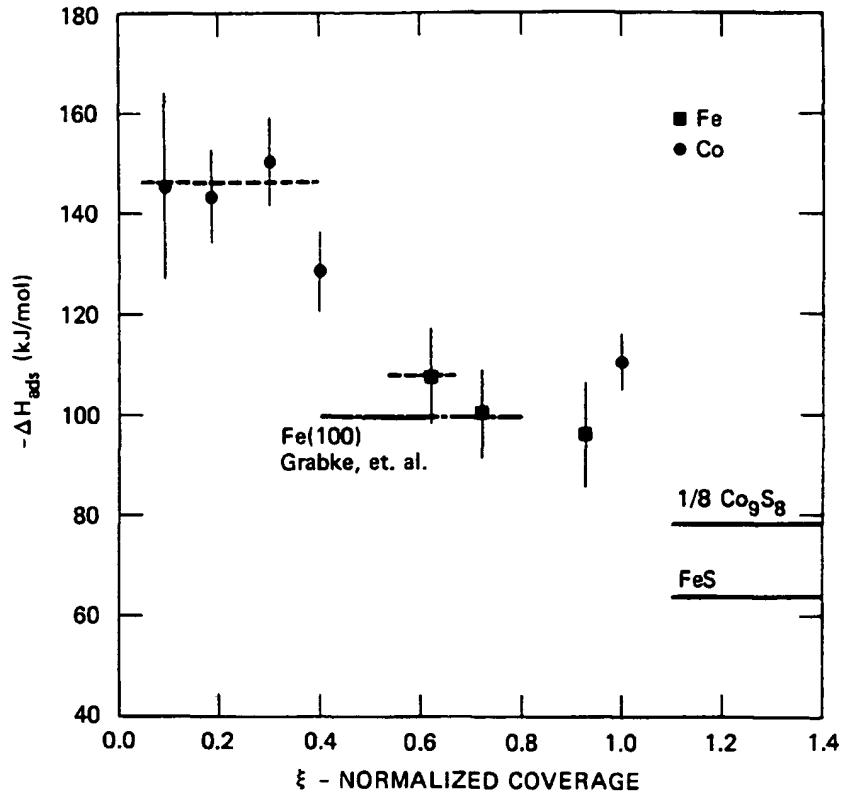

FIG. 3. Heat of sulfur chemisorption vs coverage on Fe and Co powders.

tal techniques employed. The data show that even at very high temperatures the thermodynamic activity of sulfur is extremely low for fractional coverage with chemisorbed sulfur.

It is valuable to examine the entropy of formation of chemisorbed sulfur $S_f^\circ(T)[S(a)]$. In principle this parameter can be estimated from an analysis of the vibrational modes of the adsorbed phase. However, vibrational data for sulfur adsorbed on all of the metals studied are unavailable; in addition, one needs to consider other contributions to the entropy such as adatom–substrate interactions and the configurational contributions. Nevertheless, sufficient data exist to estimate the standard entropy of formation of chemisorbed sulfur on a metal, such as nickel, and to compare it with the entropies of formation measured for Fe, Co, and Ru.

The higher frequency-stretching modes[15] for adsorbed sulfur on Ni(100) are found to be 46 meV for the $p(2\times2)$ structure, and 44 meV for the $C(2\times2)$ structure. We approximate the collective vibrational modes of sulfur chemisorbed [as $C(2\times2)$] on nickel (100) by vibrations with the frequencies 355, 258, and 135 cm^{-1}, corresponding to high resolution electron energy loss spectroscopy (EELS) peaks at 44, 32, and 16.7 meV, respectively, although we recognize that the actual surface phonon frequencies are distributed.[16] Similar vibrational modes were found for sulfur chemisorption on Ni(111).[17] Treating each mode as a one-dimensional harmonic oscillator,[18] i.e., using the Einstein model, we have calculated the vibration entropy for sulfur adatoms on Ni at 850 K and obtained a value of 48.5 $J\,mol^{-1}\,K^{-1}$. Considering the uncertainty of the atom frequency distribution, the probable variation in frequency distribution with surface structure, and the unknown changes in the substrate surface vibrational modes due to the presence of the adsorbed phase (for example, oxygen adsorption of Ni may increase the vibrational frequency of the nickel atoms at the surface),[19] we estimate that the actual vibration entropy of sulfur chemisorbed on Ni is within the range 50 ± 20 $J\,mol^{-1}\,K^{-1}$ for temperatures from 800 to 900 K. This value is somewhat less than the experimental entropies of formation for sulfur adsorbed on Ni (Table III), but is comparable to the entropies for sulfur in bulk sulfide, taken to be the difference between the standard entropies of formation of the bulk sulfide and the pure metal, i.e.,

$$S_f^\circ(T)[\text{sulfide}] = S_f^\circ(T)[\text{Me}_x\text{S}] - xS_f^\circ(T)[\text{Me}] .$$

Similar considerations apply to cobalt. However, for chemisorbed sulfur on Fe and Ru[20] the experimental entropies are significantly greater by about 30 $J\,mol^{-1}\,K^{-1}$.

The configurational contribution to the entropy of adsorption is determined by the sulfur surface coverage and the nature of the adsorption. For noninteracting adatoms with a single binding energy, the Langmuir adsorption isotherm applies, and

$$S_f^\circ(\text{config}) = -R\ln[\theta/(1-\theta)] .$$

For repulsive nearest neighbor adatom interactions, at low coverage, $S_f^\circ(\text{config}) \cong -R\ln\theta$. But as the coverage approached one-half monolayer [for a (100) surface], the configurational entropy would decline sharply until all noninteracting sites were filled. The entropy would then suddenly increase as the nearest neighbor sites started

TABLE III. Thermodynamics of sulfur chemisorption of metals.

Metal	Coverage (ξ)[a]	T_{avg}(K)	$S_f^\circ(T_{avg})[S(a)]$[b] (J mol^{-1} K^{-1}) Experimental	Calculated	$\Delta H_f^\circ(T_{avg})[S(a)]$ (kJ mol^{-1} K^{-1}) Experimental	Calculated
Ni	0.63	863	71	49	−249 ± 17	−268
	0.72	826	52	48	−248 ± 12	−251
	0.75	806	47	47	−244 ± 18	−244
	0.92	701	52	43	−216 ± 5	−222
	0.98	625	66	41	−196 ± 26	−212
	1.12	536	72	37	−174 ± 8	−193
Co	0.09	855	68[c]	55	−234 ± 18	−246
	0.18	845	69[c]	55	−233 ± 9	−245
	0.3	828	62[c]	54	−240 ± 8	−247
	0.4	844	89[c]	55	−216 ± 7	−245
	1.0	702	68	51	−199 ± 4	−211
Fe	0.6	826	105	74	−197 ± 9	−223
	0.7	725	95	72	−189 ± 9	−206
	0.9	677	86	70	−185 ± 10	−196
Ru	0.67	886	97	48	−215 ± 39	−258
	0.75	818	83	46	−213 ± 9	−243
	0.83	776	53	45	−216 ± 20	−222
	1.00	510	22	37	−187 ± 9	−179

[a] ξ: coverage normalized to CO uptake at 298 K.
[b] References for bulk sulfide data are: iron and ruthenium, Ref. 11; nickel and cobalt, Ref. 21. For ruthenium, $S_f^\circ(298)[RuS_2(s)]$ was taken as 14.5 cal mol^{-1} K^{-1}.
[c] S_f° for sulfur adsorption on cobalt has been adjusted by $+R\ln[\xi(1-\xi)]$ for $\xi \le 0.4$ to allow for configurational entropy.

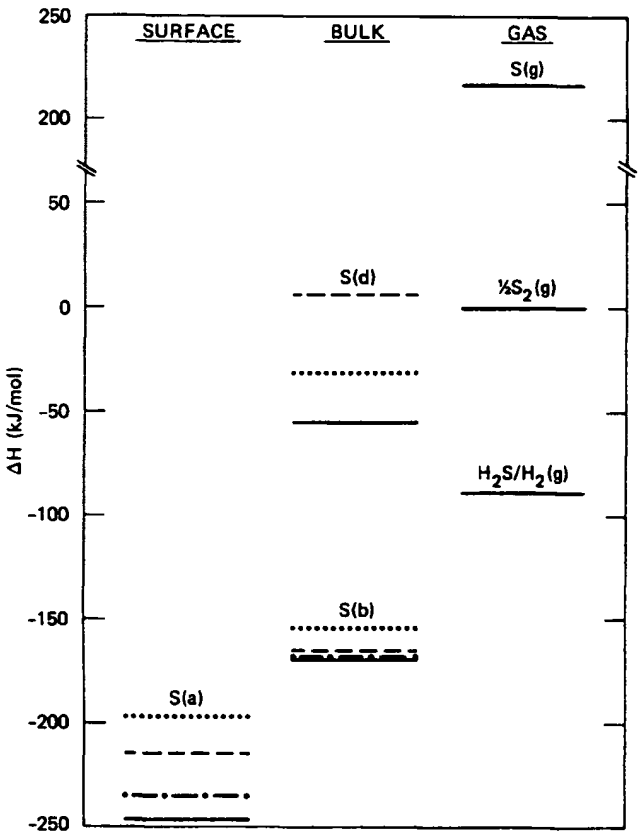

FIG. 4. Energetics of sulfur interaction with metals relative to $\frac{1}{2}$ S_2(g).

filling (at higher energy), declining again as monolayer saturation coverage was reached. For two-dimensional phase transformations, as might be expected for very attractive nearest neighbor interactions, the configurational term would vary as $-\ln\theta$ up to the nucleation point and remain nearly constant thereafter.

We conclude that the configurational entropy term for sulfur chemisorption should vary approximately as $R\ln\phi$ for $\phi \ll 0.5$ (where ϕ is the surface coverage with sulfur relative to saturation coverage). For $\phi \ge 0.5$, the S_f°(config) term is very difficult to predict since the isotherms obviously do not follow the Langmuir model. However, we were able to measure the isosteres for cobalt with sulfur coverages to less than one-tenth of the CO adsorption capacity; therefore in Table III, the Langmuir configurational entropy term was added to the estimated entropy of formation of adsorbed sulfur.

The measured magnitude of the heats of adsorption of sulfur at low coverage on the metal surfaces examined thus far follow the order Ni> Co> Ru> Fe. The free energy (ΔG°) of sulfur adsorption at low coverage on these metals at 850 K follows the same order, Ni> Co> Ru > Fe, although the difference between the ΔG_f° values for Ni, Co, and Ru is much less than that between the values of ΔH_f°. Since essentially the same degrees of freedom are lost during adsorption and during formation of bulk compounds, one can suggest[22] that S_f° for adsorption should be approximately the same as S_f° for bulk compound formation. If the entropy of adsorbed sulfur were taken equivalent to the entropy of the sulfides and the values for ΔH_f° were adjusted to keep ΔG_f° constant at

T_{ave} (Table III), the heats of formation for chemisorbed sulfur would be -254 kJ mol^{-1} for Ni, -246 kJ mol^{-1} for Co, -241 kJ mol^{-1} for Ru, and -215 kJ mol^{-1} for Fe. Again, the same order prevails, although the magnitudes of ΔH_f° would be increased for each metal.

The chemisorption of sulfur on these four metals exhibit more similarities than differences. The experimental heats of formation of sulfur adatoms (at 800 K for low sulfur coverage) are considerably below the corresponding levels for the bulk sulfides (see Fig. 4). The ΔH_f° levels for the bulk sulfides follow the same relative order as adsorbed sulfur, although the differences between Ni, Co, and Ru may not be significant for both adsorbed sulfur and bulk sulfides. The experimental entropy of adsorbed sulfur equals or exceeds that of the most stable bulk sulfide. The very large heat of segregation of dissolved sulfur to the surfaces of iron, cobalt, and nickel, in addition to the favorable entropy change, provides an energy potential of (135 ± 30 kJ mol^{-1}) for the well-known tendency of dissolved sulfur to segregate to the surfaces of these metals. (Presumably this trend applies to ruthenium as well, although the data for sulfur dissolved in Ru are lacking). The bond strength of a sulfur adatom at 800 K, i.e., the heat of adsorption from a monatomic gas, shows some variation from metal to metal, ranging from 464 kJ mol^{-1} for nickel to 414 kJ mol^{-1} for iron.

The present results are in good agreement with the correlation of Benard *et al.*[23] linking the heats of formation of two-dimensional metal–sulfur surface species to the heats of formation of the bulk sulfides. If we presume that the two-dimensional sulfide corresponds to the low coverage ($\xi \leq 0.7$) results for Ni, Fe, Co, and Ru, then our data for ΔH_f° (800 K) [S(a)] are close to the proposed trend line, which follows approximately the relation $\Delta H_f^\circ[\mathrm{S(a)}]_{2D} \cong 1.23\ \Delta H_f^\circ[(1/y)\mathrm{Me}_x\mathrm{S}_y]$, indicating that the heat of formation of chemisorbed sulfur on a metal surface is 20% to 25% greater than the equivalent heat of formation of the bulk sulfide of the metal.

[1] J. Oudar, Mater. Sci. Eng. **42**, 101 (1980).
[2] R. J. Madon and H. Shaw, Cat. Rev. **15**, 69 (1977).
[3] W. G. Fraukenburg, in *Catalysis*, edited by P. H. Emmett (Reinhold, New York, 1955), Vol. III.
[4] J. G. McCarty and H. Wise, J. Chem. Phys. **72**, 6332 (1980).
[5] J. G. McCarty and H. Wise, J. Chem. Phys. **74**, 5877 (1981).
[6] H. J. Grabke, Mater. Sci. Eng. **42**, 91 (1980).
[7] H. J. Grabke, W. Paulitschke, G. Tauber, and V. Viefhaus, Surf. Sci. **63**, 377 (1977).
[8] H. J. Grabke, E. M. Petersen, and S. R. Srinivasan, Surf. Sci. **67**, 501 (1977).
[9] H. J. Grabke, E. M. Petersen, and W. Paulitschke, Philos. Trans. R. Soc. London, Ser. A **295**, 128 (1980).
[10] P. K. Agrawal, J. R. Katzer, and W. H. Manogue, J. Catal. **69**, 327 (1981).
[11] *JANAF Thermochemical Data*, edited by D. R. Stullard and H. Prophet (Dow Chemical, Midland, Mich. 1970).
[12] K. C. Mills, *Thermodynamic Data for Inorganic Sulfides, Selenides, and Tellurides* (Butterworths, London, 1974).
[13] O. Kubaschewski and C. B. Alcock, *Metallurgical Thermodynamics*, 5th ed. (Pergamon, New York, 1979).
[14] N. Barbouth and J. Oudar, Scr. Metall. **6**, 371 (1972).
[15] S. Andersson, Surf. Sci. **79**, 385 (1979).
[16] J. E. Black, B. Laks, and D. L. Mills, Phys. Rev. B **22**, 1818 (1980).
[17] H. Ibach and D. Brushmann, Phys. Rev. Lett. **44**, 36 (1980).
[18] J. L. Hill, *An Introduction to Statistical Mechanics* (Addison-Wesley, New York, 1960).
[19] G. Allan and J. Lopez, Surf. Sci. **95**, 214 (1980).
[20] The entropy for bulk RuS_2 is very uncertain (and probably low) since it is based solely on estimated thermochemical data (see Ref. 12).
[21] I. Barin and O. Knapp, *Thermodynamic Properties of Inorganic Substances* (Springer, Berlin, 1973).
[22] N. A. Gjostein, Acta. Met. **11**, 969 (1963).
[23] J. Bernard, J. Oudar, N. Barbouth, E. Margot, and Y. Berthier, Surf. Sci. **88**, L35 (1979).

Thermodynamics of sulfur chemisorption on metals. I. Alumina-supported nickel

Jon G. McCarty and Henry Wise

Materials Research Laboratory, SRI International, Menlo Park, California 94025
(Received 28 August 1979; accepted 27 February 1980)

Sulfur chemisorption isosteres have been measured for nickel in powdered form and for nickel supported on two different alumina powders. The experiments were conducted in a closed-loop gas recirculation system containing one atmosphere hydrogen. Isotherms were determined by stepwise injection of H_2S aliquots into recirculating hydrogen gas and analyzing for the H_2S concentration as equilibrium was approached. Isosteres were measured by varying the sample temperature and monitoring the H_2S/H_2 ratio in the gaseous environment. A gas chromatograph and a photoionization detector was used to measure the H_2S concentration to levels below 1 ppb. As monolayer coverage is approached the H_2S/H_2 ratio attains the equilibrium values reported for the bulk sulfide, Ni_3S_2. Adsorbed sulfur is very strongly bound to the surface of nickel. The heat of formation of chemisorbed sulfur with respect to 1/2 $S_2(g)$ at 800 K is 247 kJ mol^{-1} more negative than the heat of formation of Ni_3S_2. The heat of segregation exceeds 190 kJ mol^{-1}. The results demonstrate that the equilibrium sulfur coverage exceeds one half monolayer on Ni/Al_2O_3 unless the H_2S/H_2 ratio is less than 1 ppb even at temperatures as high as 940 K.

I. INTRODUCTION

Nickel catalysts, presently the most suitable material for the efficient production of methane from coal-derived synthesis gas, are highly susceptible to deactivation by trace contaminants of sulfur compounds in the feedstocks. Although deactivation of nickel methanation catalysts has been observed with as little as 0.3 ppm H_2S in the inlet gas,[1] the thermodynamic aspects of sulfur poisoning on nickel have not been determined with sufficient accuracy to establish the threshold levels of sulfur contaminants above which the catalyst surface accumulates a specified fractional sulfur coverage. The purpose of the present study is to provide basic thermodynamic information relating the surface coverage of sulfur on metallic nickel crystallites to the gas phase sulfur activity in a reducing atmosphere.

The reversible adsorption of sulfur on nickel surfaces was first reported by Perdereau and Oudar[2] in 1970 for a polycrystalline foil, followed in 1971 by Rostrup-Nielsen[3] for nickel supported on $MgO \cdot Al_2O_3$. Both authors measured sulfur chemisorption isotherms with sulfur activity (defined by the ratio of H_2S to H_2) of the order 10^{-6} at elevated temperatures. These studies suggested that the free energy of formation of chemisorbed sulfur was at least 50 kJ mol^{-1} more negative than the most stable bulk sulfide Ni_3S_2.[4] Recently, Oliphant *et al.*[5] published H_2S desorption isotherms for several supported nickel catalysts. An enthalpy of adsorption of -160 kJ mol^{-1} and a free energy of formation -45 kJ mol^{-1} of chemisorbed sulfur were reported.

The present study extends the measurement of sulfur adsorption isotherms and isosteres on supported nickel surfaces to considerably lower levels of sulfur activity than previously attained. By means of a specially designed system incorporating a higher sensitivity sulfur detection device, we were able to determine reliably the equilibrium concentration of H_2S in one atmosphere of H_2 at levels below 1 ppb.

We have also examined the chemisorption of sulfur on the (100) and (111) planes of single crystal nickel using a technique similar to that of Perdereau and Oudar. The results of the study on single crystal nickel will be discussed in detail in a subsequent paper.[6]

II. EXPERIMENTAL DETAILS

System design and operation

A closed-loop gas-recirculation system has been assembled and used to measure isosteric heats of sulfur chemisorption on alumina-supported nickel crystallites and powdered nickel samples. Figure 1 is a schematic diagram of the apparatus. The heart of the apparatus is a Teflon and quartz loop, represented in Fig. 1 as a bold line. Essential equipment in the closed loop include an electrically heated quartz microreactor which retains the catalyst sample; two Teflon rotary valves, one for gas analysis (I2), the other for injecting sulfur (I3); and a Teflon diaphragm pump with a glass bulb to dampen pressure fluctuations. The loop is isolated by Teflon diaphragm valves (V8 and V9). During operation H_2S is

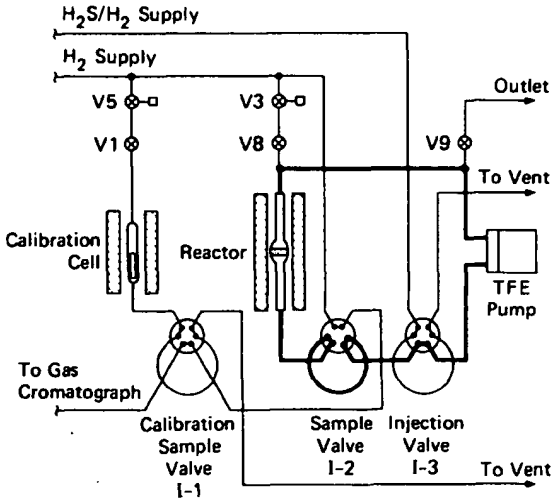

FIG. 1. Sulfur chemisorption system for dispersed metal catalysts.

 0021-9606/80/126332-06$01.00

injected into the loop and the recirculating gas is analyzed for H_2S by a special gas chromatograph column and detector.

The lower sensitivity limit of the gas chromatographic detection system is 0.1 ppb H_2S. The sensitivity is limited by baseline drift rather than noise sources. The column is a 6-ft. length of FEP tubing with 0.095 in. i.d. packed with Chromosil 310 (a treated silica gel designed to separate H_2S). The detector is a photoionization cell, HNU Model PI-51, equipped with a 10.2 eV hydrogen lamp. Both detector and column are operated at 298 K in a hydrogen carrier stream of 30–40 cm^3/s. The sampling volume is 1.26 cm^3 (I2).

For detector calibration, a solid-state electrochemical cell $Ag_2S/AgI/Ag$, generates known concentrations of H_2S in a hydrogen stream. The nonstoichiometries of the α and β forms of Ag_2S, first observed by Wagner,[7] were verified by monitoring the cell voltage and current as a function of time with the cell under vacuum. The rate of H_2S generation was limited by the kinetics of reaction of H_2 with β-Ag_2S at 410 K. Increasing the cell voltage had little effect on the rate. Application of 25 to 50 mV potential between the electrodes allowed Ag^+ ions to migrate to the Ag electrode and generate a measured electric current in the cell. The H_2S generation rate was equal to one-half the cell current inasmuch as electric leakage across the AgI ionic conductor was small at 50 mV. The cell was reliably accurate for calibration at 0.1 ppm and above.

Adsorption isotherms for the nickel–sulfur system are determined by injecting H_2S aliquots stepwise into the recirculation loop and analyzing the recirculating gas for H_2S after equilibrium is reached. After a uniform sulfur coverage is attained at the highest temperature examined for that coverage, precise isosteres are measured below 1 ppm by decreasing then increasing the catalyst temperature and monitoring the H_2S/H_2 ratio while the gas circulates over the catalyst. The coverage was considered uniform when the isosteric data points agreed for decreasing and increasing temperature. However, when the H_2S concentration exceeds 1 ppm, the recirculating gas (260 cm^3) accumulates a significant amount of sulfur, thus lowering the average sulfur coverage.

The concentration of H_2S in the recirculating gas stream can be analyzed via injection valve I2 and the gas-chromatograph column and detector. Thus, one can follow the approach to equilibrium as a function of time and thereby gain some indication of transport rates and adsorption kinetics. Because the sampling volume is small, depletion of H_2S by aliquot sampling is insignificant.

The closed-loop system places severe demands on the materials of construction. The materials must (a) be inert to irreversible H_2S adsorption and reaction, (b) have minimal sites for reversible adsorption to avoid sinks and sources of H_2S with changes in pressure, and (c) seal leak tight to prevent air diffusion into the loop or H_2 and H_2S leakage out of the loop. We decided to use a quartz reactor and to use tetrafluoroethylene polymer (TFE Teflon) and quartz as the materials of construction whenever possible because H_2S adsorbs on metal and most glasses at room temperature.[8] For sampling, six-port rotary Teflon valves (I1, I2, I3) rigged with injection loops are satisfactory. The internal components of the recirculation loop were constructed entirely of quartz and Teflon. We did not observe adsorption of H_2S when it was injected into the loop with the reactor empty. Heating the quartz bulb previously exposed to H_2S from 30 to 80 °C desorbed only 0.3 nmol H_2S. Thus, the loop was inert and had minimal H_2S adsorption capacity for 1 ppm H_2S in 1 atm H_2 at room temperature.

However, leakage or permeation in the valves and fittings allowed air to accumulate in the loop at a rate of 1 ppm/min. The H_2S partial pressure was not noticeably affected by this accumulation of air. Most likely, the oxygen that leaked into the system was converted to water. The resulting H_2O levels attained were estimated to be less than 100 ppm during measurement periods.

Interference in our measurements by atmospheric constituents at 1 ppm/min leak rates is minimal because conversion of H_2S or chemisorbed sulfur to SO_2, COS, CH_3SH, CS_2, or sulfate ion are thermodynamically unfavorable in a reducing atmosphere of H_2 at 723 K.

Catalyst preparation

Sulfur chemisorption isosteres have been measured for three nickel samples. The first was a powdered nickel sponge obtained from Johnson Matthey and Co. (spectroscopically pure). Based on CO adsorption at 300 K, the surface area of the powder was very low (0.26 m^2/g) (assuming CO saturation coverage = 1.1×10^{15} molecule/cm^2) after 120 min reduction in H_2 at 773 K. The sample continued to sinter at 773 K. After 16 h of reduction in 1 atm H_2, the specific surface area had decreased to 0.20 m^2/g.

The second sample was a 5 wt% Ni catalyst supported on alumina. The support, Condea Pural A, a high-surface-area (350 m^2/g) γ-alumina, was calcined in pure O_2 at 773 K for 60 min, and then impregnated with an aqueous solution of $Ni(NO_3)_2$ by the incipient wetness technique. The catalyst was dried in air and calcined in O_2 at 623 K for 100 min. For adsorption studies a sample (3.2 mg) was loaded into the reactor and reduced *in situ* in flowing H_2 for 750 min at 825 K. Based on CO adsorption, we estimate a specific surface area of 75 m^2/g nickel.

The third sample was Ni (5 wt%) supported on a low-surface-area alumina (20 m^2/g 65% α-alumina). The support was calcined in pure oxygen at 1100 K for 8 h, ground, screened to a mean particle size of 80 ± 20 μm, and then impregnated with $Ni(NO)_3$ solution. The catalyst sample (18.2 mg) was reduced *in situ* in pure H_2 for 15 h at 775 K and 5 h at 930 K. The specific metal surface area was 51 m^2/g, based on CO adsorption at 310 K. Table I summarizes the properties of the three nickel samples used in this study.

III. EXPERIMENTAL RESULTS

The isosteric heats for sulfur chemisorption on three nickel catalysts were determined from the adsorption

TABLE I. Nickel catalyst properties.

Catalyst	Weight (mg)	Specific surface area[a] (m^2/g) Support	Metal
Ni sponge	40	...	0.20
5 wt% Ni/γ-Al_2O_3	3.2	γ-Al_2O_3 350	75
5 wt% Ni/γ-Al_2O_3	18.2	65% α-Al_2O_3 20	51

[a]Based on CO uptake at 300 K on exposure to 1 vol% CO in He and on the assumption of 1.1×10^{15} CO adsorption sites per cm^2 of metal.

isosteres (Fig. 2). The parameter ξ represents the fractional surface coverage by sulfur relative to CO adsorption. At the sulfur coverages used in these studies, we calculate from these data the heats and entropies of adsorption (Table II), based on the equation

$$P_{H_2S}/P_{H_2}=K_p=\exp(\Delta H/RT-\Delta S/R)\,, \quad (1)$$

where ΔH and ΔS are relative to gaseous H_2S and H_2. The surface coverage ξ for the Ni sponge isostere (Fig. 2) could not be precisely determined because of the uncertainty of the degree of sintering, but it probably equals or exceeds 0.5. Despite the differences in the nature of the support, the dispersion of the nickel crystallites, and the relative sulfur coverage, the enthalpies and entropies of adsorption are the same within experimental uncertainty for the three catalysts.

A series of isosteres with increasing sulfur coverage were determined for the Ni/α-Al_2O_3 (5 wt%) catalyst (Fig. 3). The heats of adsorption calculated from the isosteres (Table III and Fig. 4) exhibit three regimes. At relatively low surface coverage of sulfur ($\xi<0.75$), the heat of adsorption has an average value of $\langle\Delta H_a\rangle_{av}=-157$ kJ mol^{-1}. At higher coverage it slowly decreases and then exhibits a discontinuous increase for $\xi>1.12$. The adsorption entropies remain nearly constant then increase discontinuously above $\xi=1.12$ (Table III), coincident with the rapid increase in ΔH_a. The discontinuity in ΔH_a and ΔS_a probably represent a change in the adsorbing species, from S adatoms to $HS(a)$ or $H_2S(a)$. At the lowest coverage, $\xi=0.63$, for which isosteres were measurable on Ni/α-Al_2O_3 (5 wt%), the sulfur activity was very low, reaching only 5 ppb at 932 K.

Adsorption isotherms were evaluated at 823, 623, and 473 K (Table IV) from the data represented in Fig. 3 for Ni/α-Al_2O_3. The equilibrium sulfur activity shows an exponential increase with increasing coverage e.g., eight orders of magnitude at 623 K. The isotherms cannot be interpreted in terms of Langmuir adsorption, i.e., sulfur adatoms bound to localized noninteracting sites.

TABLE II. Sulfur adsorption equilibria on various nickel catalysts.

Catalyst	Coverage relative to CO uptake (ξ)	Adsorption enthalpy ΔH_{ads} (kJ mol^{-1})	Adsorption entropy ΔS_{ads} J mol^{-1} K^{-1})
Ni sponge	>0.5	-143.5 ± 18.0	35.9
Ni/γ-Al_2O_3 (5.0 wt%)	0.64	-143.1 ± 16.3	39.6
Ni/α-Al_2O_3 (5.0 wt)	0.75	-155.2 ± 17.7	35.9

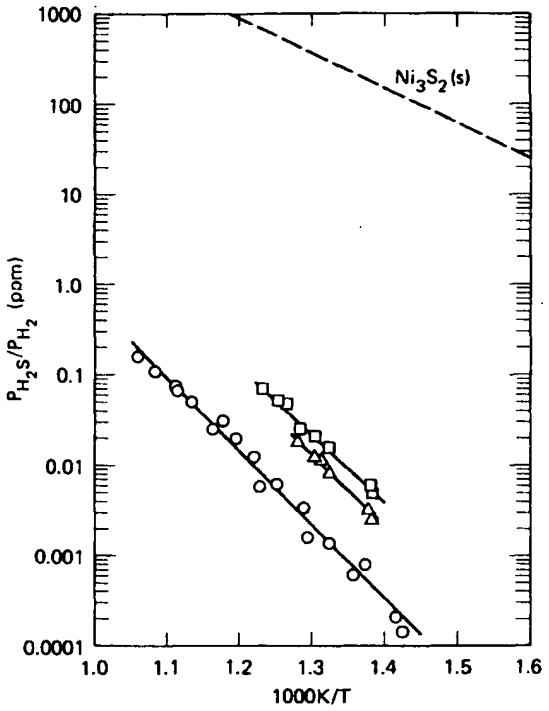

FIG. 2. Thermodynamic activity of sulfur chemisorbed on supported nickel. (o) 5 wt% Ni/α-Al_2O_3, $\xi=0.75$; (□) 5 wt% Ni/γ-Al_2O_3, $\xi=0.64$; (Δ) Ni sponge, $\xi=0.5$, where ξ is the coverage normalized to CO uptake at 300 K.

The rate of approach to equilibrium was generally slow even at temperatures as high as 900 K. After H_2S

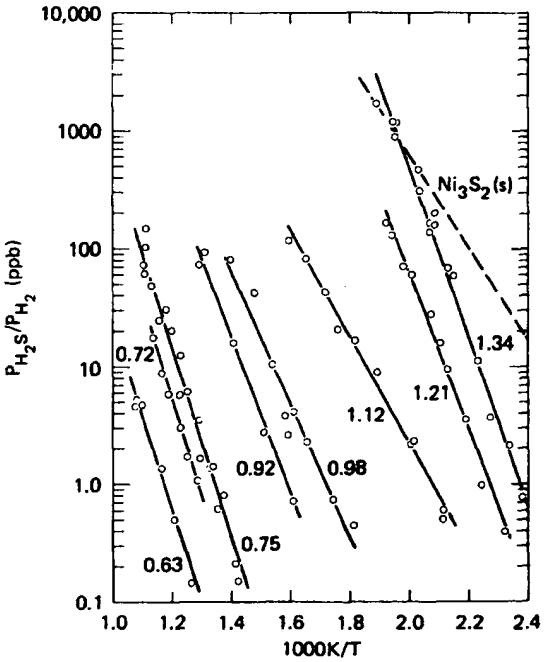

FIG. 3. Sulfur chemisorption isosteres on Ni/α-Al_2O_3 with coverage (ξ) normalized to CO uptake at 300 K.

TABLE III. H_2S/H_2 isosteres on $Ni/\alpha\text{-}Al_2O_3$ (5 wt%) catalyst (least squares analysis).

Coverage[a] (ξ)	Temperature range (K)	ΔH_f (kJ/mol)	ΔS_f (J/mol K)	r[b]	n[c]
0.63	863±70	−159.4±16.5	−13.5±19.1	0.985	6
0.72	826±50	−158.9±11.5	−32.0±13.9	0.997	6
0.75	806±125	−155.2±17.7	−35.9±22.0	0.994	19
0.92	701±74	−127.4±5.3	−30.0±7.6	0.999	5
0.98	625±85	−108.3±25.8	−13.9±41.3	0.973	9
1.12	536±75	−86.6±8.3	−7.5±15.5	0.995	10
1.21	478±45	−127.4±12.3	−117.0±25.7	0.995	10
1.35	477±50	−136.7±16.0	−152.0±33.5	0.993	17

[a]Coverage normalized to CO uptake (46 μmol/g catalyst) at 300 K.
[b]Correlation coefficient for $\ln(P_{H_2S}/P_{H_2})$ vs 1000 K/T.
[c]Number of data points in analysis.

TABLE IV. H_2S/H_2 isotherms for $Ni/\alpha\text{-}Al_2O_3$ (5 wt%) catalyst.[a]

Relative coverage[b]	P_{H_2S}/P_{H_2} (ppb) 823 K	623 K	473 K	Fractional S-saturation coverage
0.63	0.46	(4.7×10^{-4})	···	0.57
0.72	3.9	(2.3×10^{-3})	···	0.65
0.75	10.7	(7.4×10^{-3})	···	0.68
0.92	(305)	0.78	(3.2×10^{-4})	0.84
0.98	(715)	4.4	(5.9×10^{-3})	0.89
1.12	···	135	0.67	1.01
1.21	···	(26,500)	10.8	
1.35	···	(336,000)	78	

[a]Numbers in parentheses represent extrapolated values.
[b]Normalized to CO uptake (46 μmol/g catalyst) at 300 K.

was injected into the recirculating gas, no H_2S was observed to penetrate the catalyst bed when the coverage was below $\xi = 0.6$. For successively higher initial coverage, the H_2S level would quickly rise and then slowly decline with a time constant about 50 min. The decay rate decreased with the decreasing H_2S level; decay required approximately 4 h at 100 ppb and proportionately longer at lower H_2S concentration. After injection at an aliquot of H_2S, the sample was held at the highest experimental temperature for that coverage in order to speed the approach to equilibrium. Slow diffusion through the porous catalyst particles at low H_2S concentration is most likely responsible for the long times required to reach uniform coverage.

IV. DISCUSSION

The results of the present study of sulfur chemisorption thermodynamics for the $Ni/\alpha\text{-}Al_2O_3$ can be described in the following terms. At low coverage ($\xi < 0.8$) chemisorbed sulfur on nickel crystallites yields a heat of formation of -160 kJ mol^{-1} and an entropy of 30 J mol^{-1} K^{-1}. As the coverage increases, the absolute value of the heat of formation decreases because of repulsive interaction between adjacent chemisorbed sulfur atoms. The entropy of the adlayer remains unchanged (within experimental error of ±12 J mol^{-1} K^{-1}), until high sulfur coverages are attained ($0.63 < \xi \leq 1.12$). At the highest sulfur surface densities encountered in our experiments, a very large entropy change is observed (Table III). An entropy change of this magnitude is well beyond experimental error and is unlikely to be explained by configurational, structural, or vibrational contributions to the entropy of chemisorbed sulfur atoms. The isosteres at $\xi = 1.21$ and $\xi = 1.35$ probably represent adsorption of sulfur as SH adspecies or H_2S molecules on either the sulfur overlayer on nickel or on the alumina support. These isosteres were measured at low temperatures (below 525 K) where H_2S or SH adsorption is more likely to take place. Chemisorption of H_2S on γ alumina has been reported[9] with isosteric heat of adsorption of 100 to 160 kJ mol^{-1} and P_{H_2S}/P_{H_2} ratios equivalent to 1000 ppb at 525 K.

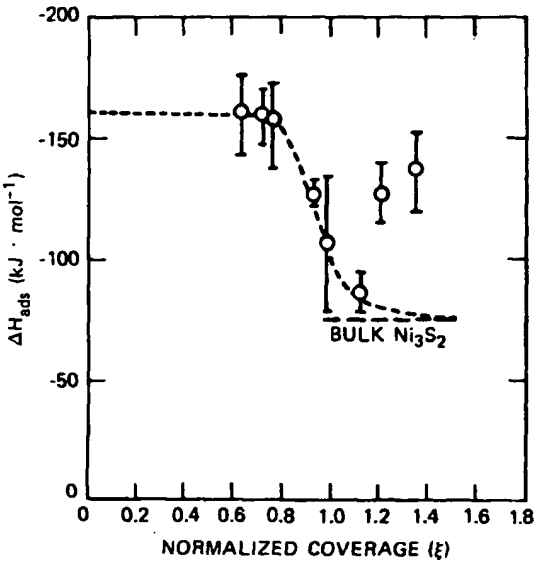

FIG. 4. Heat of adsorption of sulfur via H_2S/H_2 on $Ni/\alpha\text{-}Al_2O_3$ vs coverage (ξ) normalized to CO uptake at 300 K.

The energy of the sulfur adsorption bond to nickel surfaces is very large, approaching 465 kJ mol^{-1}, which gives rise to such well known phenomena as sulfur segregation at grain boundaries in the metallurgy of nickel and nickel alloys, and the irreversible poisoning of nickel catalysts by exposure to sulfur containing gases. The heat (enthalpy) of adsorption of sulfur on a nickel surface in equilibrium with a H_2S/H_2 mixture at a coverage well below saturation is -158 ± 9 kJ mol^{-1} at 800 K (with H_2S as the reference state for sulfur). The standard thermodynamic reference state for sulfur at this temperature is gaseous diatomic sulfur $S_2(g)$, and the heat of formation of gaseous H_2S at 800 K (Ref. 10) is -89 kJ mol^{-1}. Therefore, the heat of formation of chemisorbed sulfur is -247 ± 9 kJ mol^{-1} referenced to diatomic sulfur. The bond strength at 800 K for sulfur adatoms at half saturation coverage is -464 ± 9 kJ mol^{-1}, based on -217 kJ mol^{-1} as the heat of formation of monatomic gaseous sulfur. Bulk $Ni_3S_2(s)$ has a heat of formation[10] per mole sulfur of -154 kJ mol^{-1} at 800 K; chemisorbed sulfur is therefore 93 kJ mol^{-1} energetically more stable than the sulfur in $Ni_3S_2(s)$, as is readily apparent from Figs. 2 and 3. The heat of formation of sulfur dissolved in nickel [S(b)/Ni] has been measured[11] and was found to be -54 kJ mol^{-1} over the temperature range from 1173 to 1473 K giving a heat of segregation of -193 kJ mol^{-1} at approximately half saturation cover-

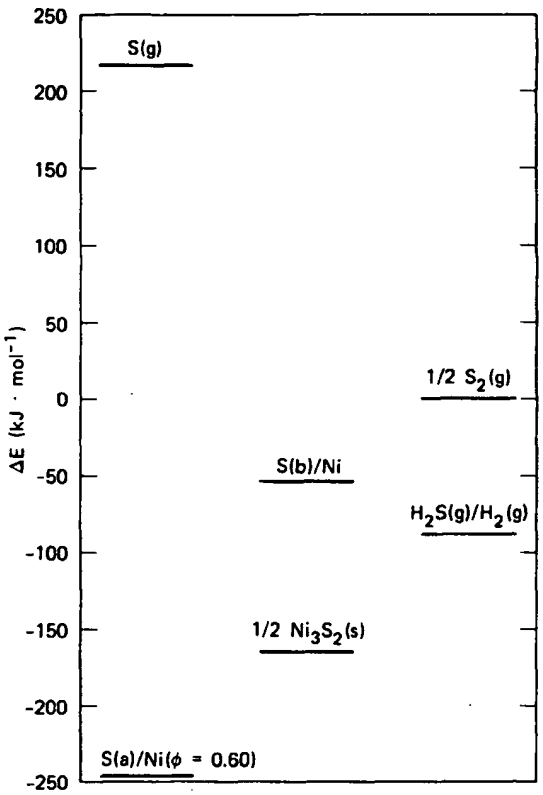

FIG. 5. Energetics of sulfur interaction with nickel at 800 K. S(*a*): adsorbed sulfur with 0.60 fractional saturation coverage (ϕ); $Ni_3S_2(s)$: bulk nickel sulfide; S(*b*): sulfur dissolved in the bulk metal; S(*g*): gaseous monatomic sulfur. The reference states are $H_2(g)$, $S_2(g)$, and Ni(*s*) at 800 K.

age. Such a large exothermic heat of segregation means that a very low level of sulfur dissolved in the bulk equilibrates with a very high surface coverage. Figure 5 summarizes the energetics of the interaction of sulfur with nickel.

The entropy of adsorption of sulfur on the Ni/α-Al_2O_3 catalyst surface at about half saturation coverage and 800 K is consistent with the entropy expected for immobile sulfur adatoms. Based on the results of the present study, the entropy change for adsorption is -27 ± 11 J $mol^{-1} K^{-1}$, which gives 56 ± 11 J $mol^{-1} K^{-1}$ as the net increase in entropy due to the presence of chemisorbed sulfur on surfaces of the nickel crystallites. Recently, Anderson[12] has measured the frequency of vibration of sulfur adatoms perpendicular to the Ni(100) surface using low energy elastic loss spectroscopy (ELS). ELS is believed[13] to excite only vibrational modes parallel to the incident beam of electrons [in this case normal to the (100) surface]. For this mode, Anderson found a vibrational wave number of 355 cm^{-1}. At 800 K, a vibrational mode of this magnitude would contribute 12 J $mol^{-1} K^{-1}$ to the entropy of chemisorbed sulfur or 37 J $mol^{-1} K^{-1}$ if all three vibrational modes have a frequency of 355 cm^{-1}. This leaves only 19 ± 11 J $mol^{-1} K^{-1}$ to be accounted for by contributions from configuration and other vibrational components. Erley *et al.*[14] have reported an ELS frequency of 390 cm^{-1} for sulfur chemisorption on Ni(111), a value that gives nearly the same vibrational contribution to chemisorption entropy as determined for Ni(100).

The magnitude of the observed entropy change from adsorption of sulfur on nickel surfaces in equilibrium with gaseous H_2S/H_2 gas mixtures rules out H_2S and SH as the adsorbed species at moderate coverage. At 800 K, we would expect to observe roughly -180 and -100 J $mol^{-1} K^{-1}$ for ΔS of chemisorbed H_2S and HS species, respectively. These values are clearly beyond the experimental uncertainty. However, at 500 K, we would expect $\Delta S = -190$ and -120 J $mol^{-1} K^{-1}$, respectively, for chemisorbed H_2S and HS. We note that the entropy change for the SH species is closer to the observed value, -135 ± 25 J $mol^{-1} K^{-1}$, at high coverage (Table III).

The results of our study of the thermodynamics of sulfur chemisorption on powdered nickel, γ-Al_2O_3-supported nickel, and α-Al_2O_3-supported nickel show that sulfur is an even more tenaciously bound catalyst poison for nickel than previously suspected. At 575 K, a typical temperature for catalytic methanation of synthesis gas, our data gives 0.7 ppb H_2S in 1 atm H_2 as the equilibrium sulfur activity at 90% saturation coverage. Thus, to prevent sulfur accumulation on the catalyst the upper limit of H_2S in syn gas for methanation is extremely low. At the same time regeneration of a sulfur-poisoned catalyst by hydrogen reduction is impractical because of the low equilibrium partial pressure of H_2S. A prohibitive volume of H_2 would be required at temperatures below 700 K to remove chemisorbed sulfur from nickel surfaces. At higher temperatures Ni crystallite sintering would become a problem.

In order to compare our isosteric results with previous measurements,[2,3,5] we need to establish reference points for the surface coverage of sulfur on different Ni surfaces and topographies. Perdereau and Oudar[2] reported that the saturation sulfur coverage on nickel surfaces (800 ppm H_2S in H_2 at 875 K after 2700 s exposure) remains nearly constant ($8.2 \pm 0.3 \times 10^{14}$ atoms per cm^2), regardless of orientation of the crystal plane. For Ni(100) single crystal planes the saturation coverage is 8.0×10^{14} atoms per cm^2, which represents 50% of the density of nickel atoms at the surface (15.9×10^{14} atoms per cm^2). This result is consistent with the C(2×2) LEED pattern observed[2,15] for saturation with sulfur on

TABLE V. Saturation coverage for sulfur chemisorption on nickel.

Material	T (K)	P_{H_2S}/P_{H_2} (ppm)	S/H[a]	Ref.	Equivalent[b] ξ - S/CO
Ni foil	1173	100	···	2	1.02
Ni foil	1073	150	···	2	1.12
Ni foil	973	150	···	2	1.13
Ni/MgO · Al_2O_3	918	8	0.74	3	1.00
Ni/MgO · Al_2O_3	823	2	0.74	3	1.05
Ni powder	723	25	1.14	5	1.15
3 wt% Ni/Al_2O_3	723	25	1.04	5	1.15
16 wt% Ni–0.5 wt% Pt/Al_2O_3	723	25	0.82	5	1.15
16 wt% Ni–0.5 wt% Pt/Al_2O_3	793	25	0.74	5	1.14

[a]Saturation S coverage vs H_2 chemisorption from reference.
[b]ξ equivalent S coverage vs CO chemisorption, this work.

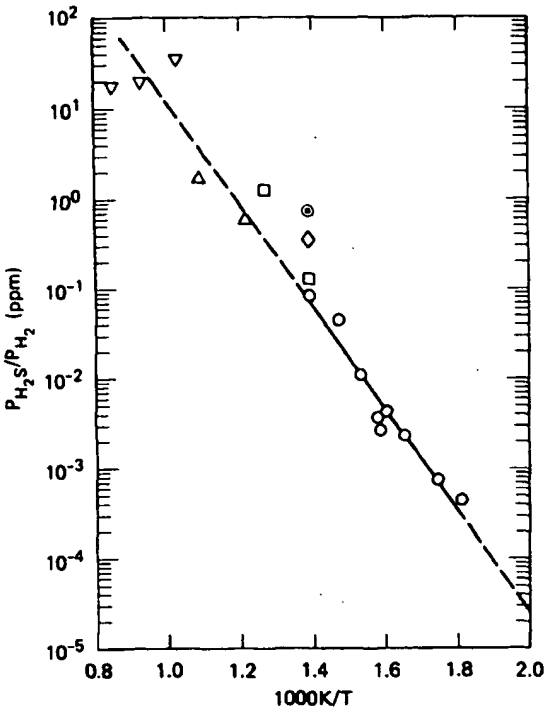

FIG. 6. Sulfur activity vs reciprocal temperature for chemisorbed sulfur. (▽) Ni foil (Ref. 2); (△) $Ni/MgO_3 \cdot Al_2O$ (Ref. 3); (●) Ni powder (Ref. 5); (◇) Ni/Al_2O_3 (Ref. 5); (□) $Ni-Pt/Al_2O_3$ (Ref. 5); (○) Ni/α-Al_2O_3 (this work); (—) least squares analysis (this work). All points are for fractional saturation coverage (ϕ) = 0.88.

the Ni(100) plane. A number of other workers[16–20] report similar values for H_2S adsorption at 200 to 300 K on nickel films and supported nickel.

However, in the determination of the surface site density on Ni surfaces by means of H_2 or CO adsorption, the adsorption stoichiometries are not firmly established beyond a factor of 2. Rostrup-Nielsen,[3] using a H/Ni(s) = 0.73, arrived at a value of S/Ni(s) = 0.54 at saturation coverage on $Ni/MgO \cdot Al_2O_3$. Based on an average surface site density of 15.4×10^{14} Ni atom/cm^2 for the low index planes of Ni, the sulfur saturation density (8.3×10^{14} S atom/cm^2) so calculated is in good agreement with Perdereau's results (8.2×10^{14} S atom/cm^2). By contrast the results of Pannell *et al.*,[21] in which H/Ni(s) is assumed to be unity, yields sulfur saturation coverage corresponding to 11.4×10^{14} S atom/cm^2 for powdered Ni and 17.6×10^{14} S atom/cm^2 for the alumina-supported Pt-promoted Ni catalyst (16 wt% Ni, 1.5 wt% Pt).

In our work CO adsorption was employed as a measure of Ni surface site density. On well defined Ni planes CO adsorption studies[22–26] gave nearly constant saturation coverage, corresponding to $11.0\pm0.3\times10^{14}$ CO molecules/cm^2 regardless of crystal orientation. Based on CO adsorption we arrive at a sulfur saturation coverage corresponding to $12.2\pm0.8\times10^{14}$ S atoms/cm^2 on 5 wt% $Ni/\alpha-Al_2O_3$. On the basis of the resulting adsorption ratio S/CO = 1.11 we have evaluated the fractional sulfur saturation coverage (ϕ) for this catalyst (Table IV), and the equivalent saturation coverage corresponding to saturation conditions used in previous work (Table V).

Now we are in a position to compare the results reported by various authors with our S chemisorption isosteres. In Fig. 6 we have plotted the data near saturation coverage ($\phi = 0.88$). It will be noted that over a wide range of temperatures the various data points are in satisfactory agreement with our results represented by the solid line. However, a similar comparison at lower S coverage ($\phi = 0.7$) demonstrate that our equilibrium H_2S/H_2 partial pressure ratios are considerably lower than those reported previously.[2,3] Based on our observation that the approach to equilibrium is very slow at low H_2S concentration, we suggest that equilibrium may not have been reached in the earlier studies.

ACKNOWLEDGMENTS

This work was supported by a grant from the Office of Basic Energy Sciences of the U.S. Department of Energy. The authors also are grateful to Professor C. H. Bartholomew (Brigham Young University), Professor M. J. Oudar (CNRS, Paris), and B. J. Wood for helpful discussion during the course of this investigation.

[1] A. L. Hansberger, C. B. Knight, and K. Atwood, in *Methanation of Synthesis Gas*, edited by L. Seglin (American Chemical Society, Washington, D. C., 1975), pp. 53–58.
[2] M. Perdereau and J. Oudar, Surf. Sci. 20, 80 (1970).
[3] J. R. Rostrup-Nielsen, J. Catal. 21, 171 (1971).
[4] T. Richardson, J. Iron Steel Inst. London 187, 37 (1954).
[5] J. L. Oliphant, R. W. Fowler, R. B. Pannell, and C. H. Bartholomew, J. Catal. 51, 229 (1978).
[6] J. G. McCarty, H. Wise, and B. J. Wood (to be published).
[7] C. Wagner, J. Chem. Phys. 21, 1819 (1953).
[8] R. K. Stevens, J. D. Mulik, A. E. O'Keefe, and K. J. Krost, Anal. Chem. 43, 827 (1971).
[9] A. J. deRosset, C. G. Finstrom, and C. J. Adams, J. Catal. 1, 235 (1962).
[10] D. R. Stull, *JANAF Thermochemical Tables* (National Bureau of Standards, Washington, D.C., 1966).
[11] N. Barbouth and J. Oudar, C. R. Acad. Sci. Ser. C 269, 1618 (1969).
[12] S. Anderson, Surf. Sci. 79, 385 (1979).
[13] H. Ibach, H. Hopster, and B. Sexton, Appl. Surf. Sci. 1, 1 (1977).
[14] W. Erley, H. Ibach, S. Lehwald, and H. Wagner, Surf. Sci. 83, 585 (1979).
[15] T. Edmonds, J. J. McCarroll, and R. C. Pitkethly, Ned. Tijdschr. Vacuumtech. 8, 162 (1970).
[16] J. M. Saleh, C. Kemball, and M. W. Roberts, Trans. Faraday Soc. 57, 1771 (1961).
[17] J. C. Muller and R. Gilbert, Bull. Soc. Chim. France 2129 (1967).
[18] I. E. Den Besten and P. W. Selwood, J. Catal. 1, 93 (1962).
[19] B. G. Martin and B. Imelik, Surf. Sci. 42, 157 (1974).
[20] J. Barcicki, J. Borowiecki, and A. Denis, Przem. Chem. 54, 234 (1975).
[21] R. B. Pannell, K. S. Chung, and C. H. Bartholomew, J. Catal. 46, 340 (1977).
[22] K. Klier, A. C. Zettlemoyer, and H. J. Leidheiser, J. Chem. Phys. 52, 589 (1970).
[23] J. C. Tracy, J. Chem. Phys. 56, 2736 (1972).
[24] H. H. Madden, J. Kuppers and G. Ertl, J. Chem. Phys. 58, 3401 (1973).
[25] H. Conrad, G. Ertl, J. Kuppers, and E. E. Latta, Surf. Sci. 57, 475 (1976).
[26] J. L. Falconer and R. J. Madix, Surf. Sci. 48, 398 (1975).

ELSEVIER

Solid State Ionics 132 (2000) 261–269

SOLID STATE IONICS

www.elsevier.com/locate/ssi

The poisoning effect of sulfur-containing impurity gas on a SOFC anode: Part I. Dependence on temperature, time, and impurity concentration

Yoshio Matsuzaki*, Isamu Yasuda

Fundamental Technology Laboratory, Tokyo Gas Co., Ltd. 16-25 Shibaura, 1-Chome, Minato-ku, Tokyo 105-0023, Japan

Received 24 December 1999; received in revised form 31 January 2000; accepted 14 February 2000

Abstract

The poisoning effect of a sulfur-containing impurity on the electrochemical oxidation of H_2 has been studied at 1023–1273 K in a gas mixture of H_2 and H_2O at the interface between a Ni–YSZ cermet electrode and a YSZ electrolyte using a complex impedance analysis and a DC polarization method. The polarization resistance and the overvoltage of the electrode increased when the H_2S concentration exceeded 0.05, 0.5, and 2 ppm at 1023, 1173 and 1273 K, respectively. A large temperature dependence was observed, which insists that a high-grade desulfurization is necessary at lower operating temperatures. The time needed for the influence of the sulfide impurity to saturate was almost independent of the sulfide concentration, and was found to be approximately 12, 9 and 4 ks at 1023, 1173 and 1273 K, respectively. Within the present experimental conditions, the performance loss caused by the sulfur-poisoning was recoverable when the sulfur source was removed from the fuel; the time needed for the recovery was approximately 360, 90 and 4 ks at 1023, 1173 and 1273 K, respectively. The degree of sulfur-poisoning was found to depend not on the equilibrium partial pressure of S_2 but on the total sulfur content in the fuel.

Keywords: Solid oxide fuel cell; Fuel electrode; Sulfur; Poisoning; Impurity; Complex impedance

1. Introduction

Fuel cells have high fuel-to-electricity conversion efficiencies and low levels of NO_x and SO_x emission. Solid oxide fuel cells (SOFCs) have attracted much attention because of their distinguished advantages over other types of fuel cells such as high electric efficiency, high-quality exhaust heat and system compactness. High operating temperatures of SOFCs ranging from 873 to 1273 K enables them to use a wide variety of fuels including natural gas. For natural gas fueled SOFCs, however, the effect of sulfide impurities must be taken into account and desulfurization was considered since several parts per million (ppm) of sulfur-containing impurities are usually added as odorant to natural gas distributed to customers by pipelines.

Among several types of SOFCs, electrolyte-supported cells using yttria-stabilized zirconia (YSZ) as the electrolyte have many material problems remain-

*Corresponding author. Tel.: +81-3-5484-4826; fax: +81-3-3453-7583.

E-mail address: matuzaki@tokyo-gas.co.jp (Y. Matsuzaki).

0167-2738/00/$ – see front matter
PII: S0167-2738(00)00653-6

ing to be solved which arise from the high operating temperature, typically around 1273 K. A reduction in the operating temperature leads to the benefits which include low-cost metallic separators instead of more expensive ceramic ones [1], better long-term performance stability, and system compactness by reducing the thickness of the heat insulator. Fundamental research, therefore, has been carried out on manufacturing and testing the cells reduced-temperature operation using electrode-supported cells [2–5] with a thin YSZ electrolyte film on thick porous electrodes as well as the electrolyte-supported cells in which the high oxide-ion conductor of doped $LaGaO_3$ is used as the electrolyte [6–8].

Although many benefits are expected by reducing the operating temperature, it should be considered that at reduced temperatures sulfide impurities may easily adsorb on the surface of a SOFC fuel electrode to degrade the resistance of the electrode against the sulfide impurities. Of impurities in fuels, the sulfur-containing compounds, which are present primarily as hydrogen sulfide (H_2S) under the fuel electrode environment are expected to have the greatest impact on SOFC performance [9].

In previous studies on the poisoning effect of sulfur, a direct-current polarization method and complex impedance analysis were used to evaluate cell performance loss, which showed that even low levels in ppm of H_2S may cause significant performance losses at the fuel electrode of SOFC. Geyer et al. [10] reported that the polarization resistance of a cermet electrode increased by a factor of two by addition of only 5 ppm of H_2S at 1223 K in H_2 with 3% H_2O. If the H_2S content is low, however, the performance recovers upon removing the sulfur impurity from the fuel [11–13]. As for the high levels of H_2S concentration, Dees et al. [14] reported that the polarization resistance increased by a factor of two by addition of 105 ppm H_2S at 1273 K in H_2 with 3% H_2O and the poisoning effect was irreversible. Several possible mechanisms may account for the decrease in the performance of the electrode due to the presence of H_2S in the fuel. The exact mechanism responsible for the performance loss, however, is not clearly defined because of the lack of detailed experimental data. In this study, we have investigated the time-constant of sulfur saturation and removal, and the dependence of the poisoning effect on the operating temperature, the sulfur contaminant concentration and the equilibrium partial pressure of S_2 produced in fuels containing H_2S.

2. Experimental

2.1. Test cell preparation

Dense pellets (20 mm in diameter and 2 mm in thickness) of 8 mol% YSZ were used as the electrolytes for electrochemical cells. NiO powder with an average grain size of 0.9 μm (Nihon-Kagaku-Sangyo) was dispersed in a mixed toluene solution of zirconium octylate ($Zr(C_4H_9CH(C_2H_5)CO_2)_4$, 99% pure, Nihon-Kagaku-Sangyo) and yttrium octylate ($Y(C_4H_9CH(C_2H_5)CO_2)_3$, 99% pure, Nihon-Kagaku-Sangyo), the mixing ratio of which was adjusted to the ratio corresponding to the composition of 8 mol% Y_2O_3–92 mol% ZrO_2. The paste thus prepared was screen-printed onto one side of the electrolyte pellet, followed by firing at 1723 K for 7.2 ks to obtain a porous NiO–YSZ composite [15]. The thickness and porosity of a Ni–YSZ cermet electrode obtained after reduction of the NiO–YSZ composite were about 25 μm and 45%, respectively. The YSZ content in the cermet electrode is 10 wt%. For a counter electrode, Pt paste (Tokuriki Kagaku 8103) was painted symmetrically to the Ni–YSZ cermet electrode on the other side of the pellet and fired at 1273 K for 7.2 ks. For a reference electrode, the Pt paste was painted at the perimeter of the pellet and fired at 1273 K for 7.2 ks.

2.2. Electrochemical measurement

Fig. 1 shows the test geometry used in the electrochemical measurements. Two Sr-doped $LaCrO_3$ plates with grooves were used as both manifolds and current collectors. Humidified H_2 fuel was fed into the doped $LaCrO_3$ plates from the top of a furnace and was supplied to the reference, counter and the Ni–YSZ cermet electrode. H_2S was added to the fuel as the sulfide impurity at the concentration range from 0.02 to 15 ppm. Platinum wires were used as voltage terminals for the working and reference electrodes.

The complex impedance measurements were made

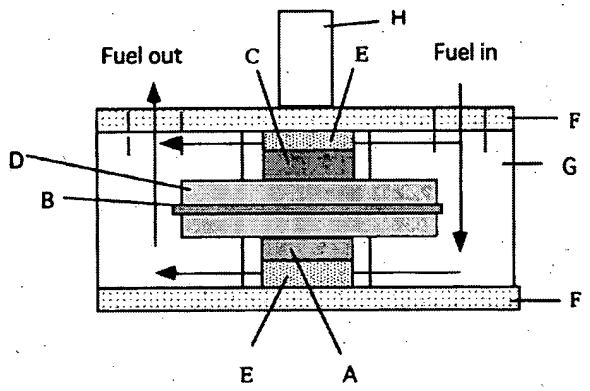

Fig. 1. Test geometry used in the electrochemical measurements. A: working electrode, B: reference electrode (Pt), C: counter electrode (Pt), D: YSZ pellet, E: Pt mesh for current collection, F: doped $LaCrO_3$ plate for current collection and manifold, G: Al_2O_3 plate for manifold, H: pushrod.

over the frequency range of 1 mHz–100 kHz with an applied amplitude of 10 mV using the three-terminal method at an equilibrium potential. The system for the impedance measurements was composed of a frequency response analyzer (Solartron 1260), a potentiostat (Solartron 1287) and a personal computer (Compac Armada I 120T). In order to keep the electrode stable during the complex impedance measurements, the electrode was pretreated under a DC polarization at the current density of 0.3 A cm^{-2} in the fuel without H_2S for 180 ks followed by annealing for 180 ks at the equilibrium potential at each temperature. The steady-state polarization was measured by a current interruption method using a current-pulse generator (Hokuto Denko HC-110). Also before the polarization measurements, pretreatment was conducted at current density of 0.3 A cm^{-2} in the fuel without H_2S for 180 ks.

3. Results and discussion

3.1. Poisoning by sulfur and recovering at 1273 K

Fig. 2 shows the change in the complex impedance spectrum with time when H_2S is added to the fuel, 79% H_2 + 21% H_2O, at 1273 K. The H_2S concentration, $C(H_2S)$, was set at 1, 2, 4, 6, 8, 10 and 15 ppm, and the impedance measurements were repeated consecutively until the spectra showed no change with time. The figure shows the four selected time-evolutions of the impedance spectra. Two arcs seemed to be overlapped in the impedance plots which show depressed semi-circles. As shown in these figures, the addition of H_2S did not change the size of impedance arcs at the concentration of 1 ppm, but increased the size of impedance arcs at 2 ppm and more. These results indicate that the Ni–YSZ cermet electrode was degraded by the sulfide impurity when the value of $C(H_2S)$ exceeded 2 ppm at 1273 K. It is found that the size of impedance arcs initially increased with time at $C(H_2S)$ of 2 ppm or more and saturated at time between 3.6 and 4.8 ks after the H_2S addition. Fig. 3 shows the complex impedance spectra after full equilibration with the fuels with several concentrations of H_2S. The steady-state impedance curves became larger with increase of $C(H_2S)$, but no significant difference appeared in the shape of the curves even when $C(H_2S)$ increased. Fig. 4 shows the change of the complex impedance spectra after the fuel with 15 ppm H_2S was switched to a H_2S-free fuel. The time in the legend is the time elapsed after H_2S was removed from the fuel. It is found that the size of the impedance arcs decreased with time and recovered to its original level at about 3.6 ks after the H_2S removal. The complex impedance spectra of the electrode equilibrated in the fuel with 2–10 ppm H_2S were also found to recover to the original size and shape at about 3.6 ks after the H_2S was removal. From these results it is concluded that 2–15 ppm H_2S impurity deteriorates the electrode at 1273 K, but this poisoning effect is reversible if the H_2S-free fuel is supplied again.

Fig. 5 shows the overvoltage (with IR) of the electrode as a function of time at the current density of 0.3 A cm^{-2} (a) and (b) show the overvoltage after H_2S was added to the fuel and H_2S was removed from the fuel, respectively. The overvoltage started to increase with time when H_2S was added to the fuel and saturated after a sufficient time; the steady-state overvoltage was larger than that in the H_2S-free fuel by about 2 mV at $C(H_2S)$ of 2 ppm and 74 mV at $C(H_2S)$ of 15 ppm. The degraded electrode performance fully recovered upon switching to the H_2S-free fuel. These results are consistent with the results in the polarization resistance evaluated by the complex impedance analysis.

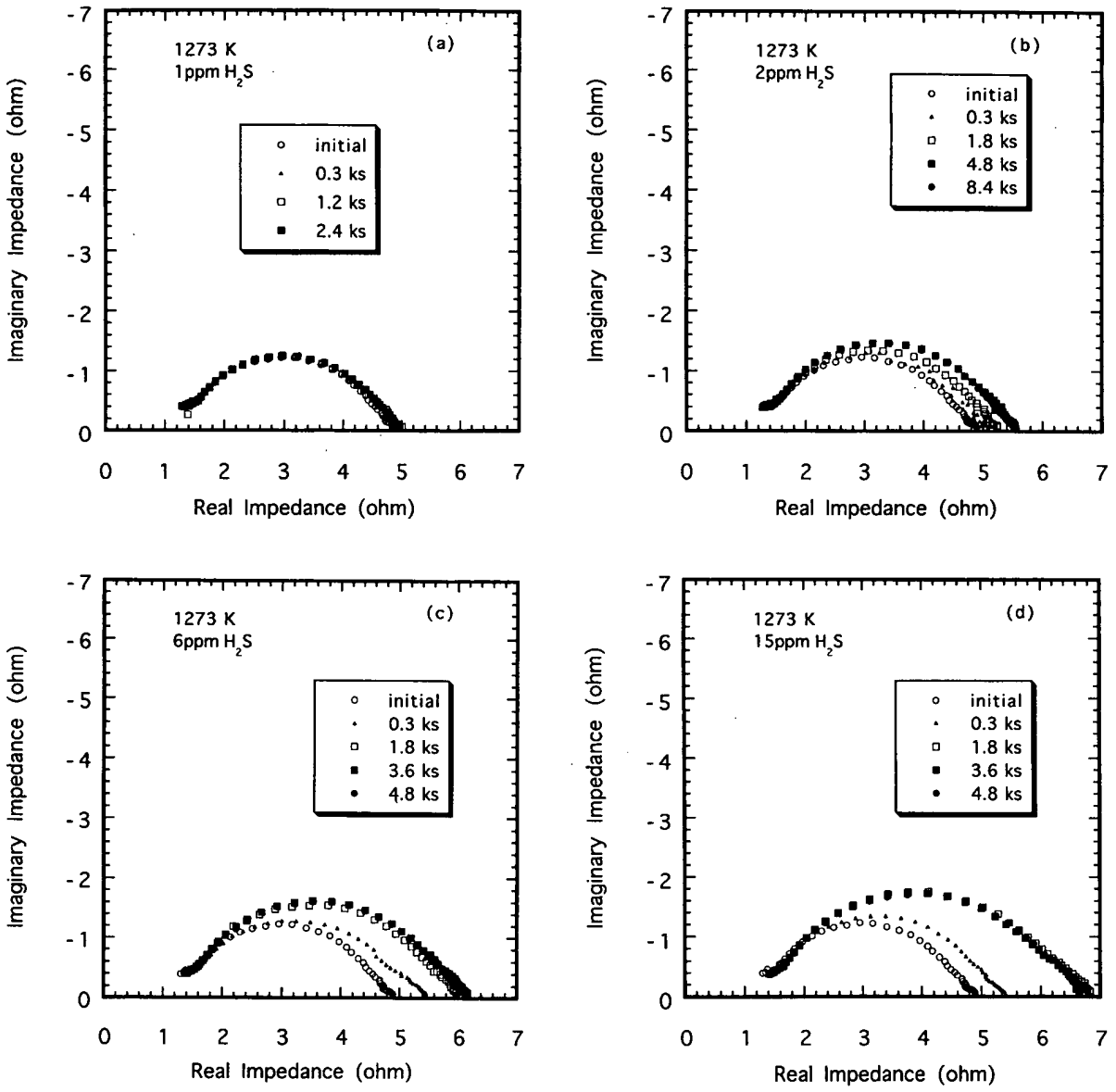

Fig. 2. The frequency dispersion diagram of the complex impedance spectra of the electrode in the fuel with H_2S of (a) 1, (b) 2, (c) 6 and (d) 15 ppm at 1273 K.

3.2. Temperature dependence of sulfur poisoning

Fig. 6 (a) and (b) show the complex impedance spectra after equilibration in the fuels with different H_2S concentrations at 1173 and 1023 K, respectively. At 1173 K, the impedance arcs increased when the $C(H_2S)$ exceeded 0.5 ppm, which was lower than that 2 ppm at 1273 K. At 1073 K the impedance arcs began to increase at a much lower concentration of 0.05 ppm. These results suggest that reducing the operating temperature degrades the resistance of the electrode against the sulfide impurities to cause the poisoning at lower sulfur concentrations.

Fig. 7 shows typical impedance spectra measured

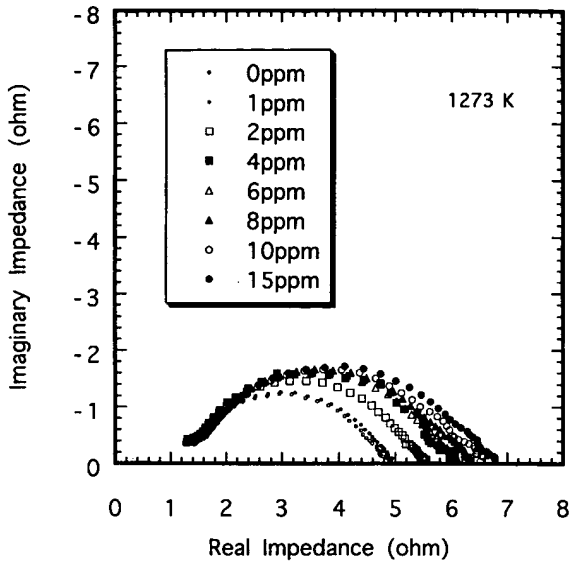

Fig. 3. The complex impedance spectra measured after equilibration in the fuels with several concentrations of H_2S at 1273 K.

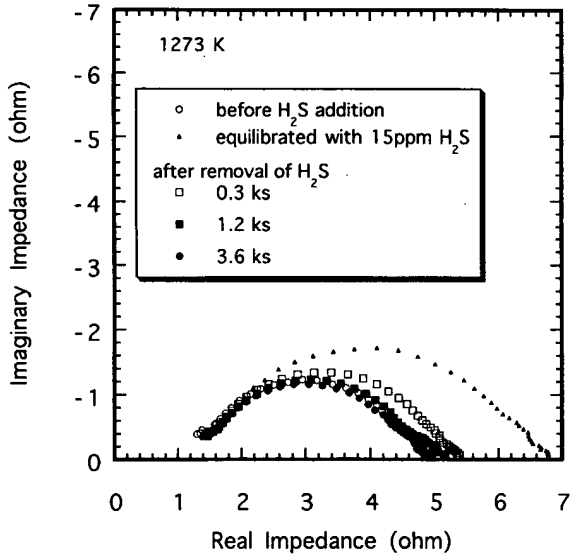

Fig. 4. The change of the complex impedance spectra at 1273 K when 15 ppm H_2S was removed from the fuel.

at 1173 K; (a) and (b) show the change of impedance spectra after addition and removal of 1 ppm H_2S, respectively. When the H_2S was added to the fuel, the size of the impedance arcs increased with time and saturated after approximately 9 ks which was longer than at 1273 K. When H_2S was removed from the fuel, the size of the impedance arcs decreased with time and finally recovered to its original level before the poisoning. However, a longer time, approximately 90 ks was needed for the recovery at 1173 K as compared with that at 1273 K, which became more remarkable at a lower temperature. The typical impedance spectra measured at 1023 K are shown in Fig. 8(a) and (b). At 1023 K, it took approximately 12 ks for the size of the impedance arcs to saturate after the H_2S addition and took approximately 360 ks for the recovery after removing H_2S. It is also found that the recovered impedance arc is smaller than that before H_2S addition, the cause of which has not yet been identified.

Fig. 9 shows the difference between the steady-state overvoltage in the fuel with the H_2S impurity and the initial overvoltage without H_2S impurity as a function of $C(H_2S)$ and the operating temperature at the current density of 0.3 A cm^{-2}. The minimum concentrations of H_2S which caused the increase of the overvoltage showed good correspondence to those for the polarization resistance evaluated by the complex impedance analysis, i.e. 2, 0.5 and 0.05 ppm at 1273, 1173 and 1023 K, respectively. Similar to the results in the complex impedance measurements, the increase in the overvoltage recovered at all temperatures when $C(H_2S)$ returns to 0 ppm, i.e. the poisoning effect of sulfur on the overvoltage is also reversible over the concentration range studied.

The degree of the poisoning caused by sulfur was thus found to have a large dependence on the operating temperature; the critical sulfur level for the performance loss is lower at lower operating temperatures, and at a selected sulfur concentration, the overvoltage increases more largely at lower temperatures. Since it can be presumed that the sulfur impurity adsorbs more easily on the electrode as temperature decreases, these results suggest that an adsorbed impurity inhibits some processes in electrochemical reactions at the interface between the fuel electrode and the electrolyte.

3.3. Dependence on S_2 partial pressure

The partial pressure of S_2, $P(S_2)$, in the fuel is determined by the following equilibrium reactions as a function of H_2 partial pressure, $P(H_2)$, $C(H_2S)$ and temperature.

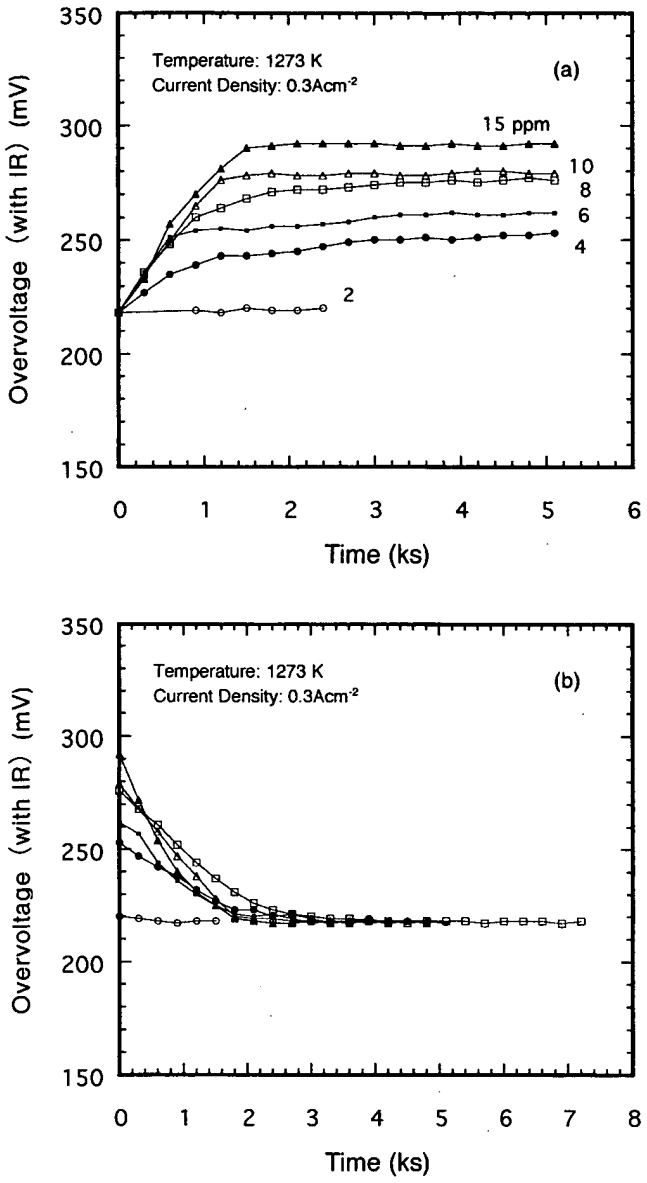

Fig. 5. The overvoltage (with IR) of the electrode as a function of time at a current density of 0.3 A cm^{-2} after (a) addition and (b) removal of H_2S.

$$2H_2S = 2H_2 + S_2 \quad (1)$$

Since $P(H_2)$ in the fuel is determined by the following equilibrium reaction as a function of the partial pressure of H_2O, $P(H_2O)$, and the partial pressure of oxygen, $P(S_2)$ is also a function of these partial pressures.

$$2H_2O = 2H_2 + O_2 \quad (2)$$

To discuss the influence of $P(S_2)$ on the sulfur poisoning of the electrode, we measured the steady-state polarization as a function of $P(S_2)$ which was controlled by changing $P(H_2O)$ with constant $C(H_2S)$ or by changing $C(H_2S)$ with constant

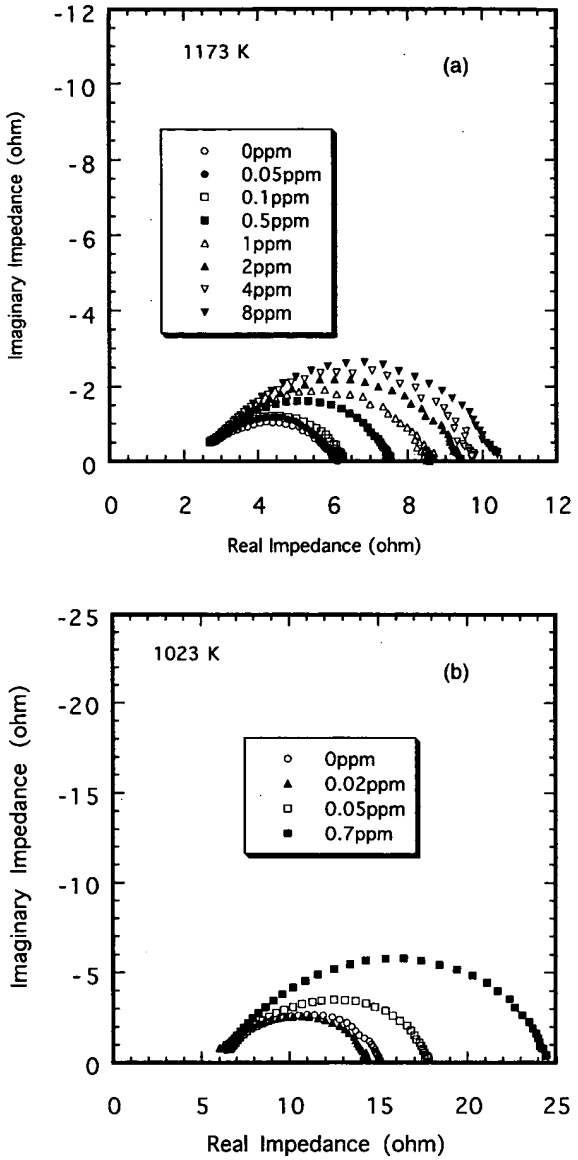

Fig. 6. The complex impedance spectra measured after equilibration in the fuels with several concentrations of H_2S at (a) 1173 K and (b) 1023 K.

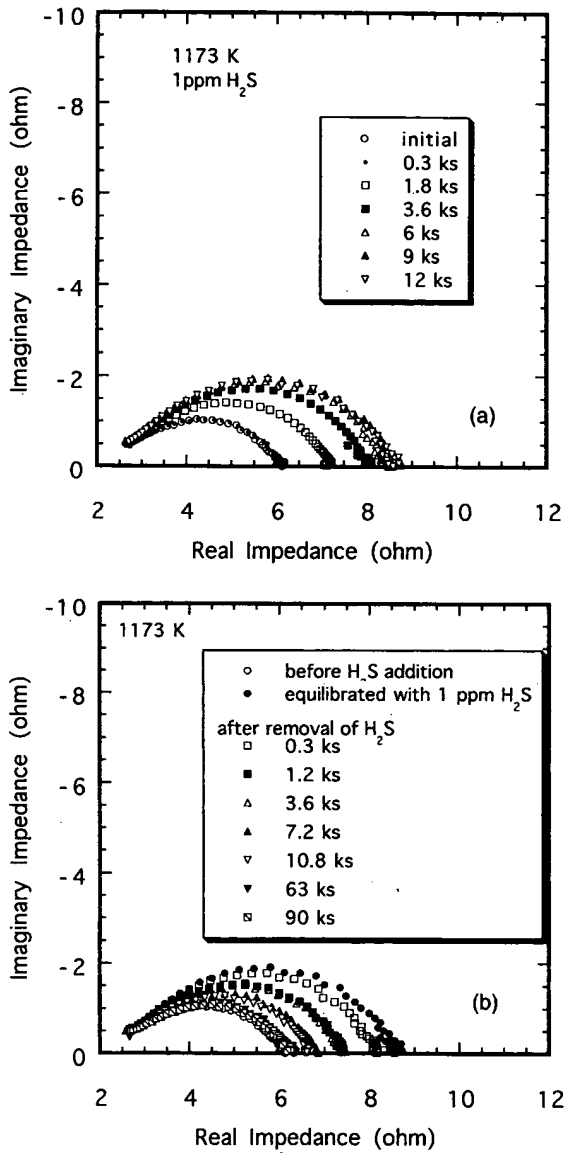

Fig. 7. Typical complex impedance spectra measured at 1173 K after (a) addition and (b) removal of 1 ppm H_2S.

$P(H_2O)$. Fig. 10 shows the increase of the overvoltage, ΔV, by the poisoning as a function of $P(S_2)$ at the current density of 0.3 A cm^{-2}. The closed circles indicate plots with constant $P(H_2O)$ with the value of 21% at all temperatures. With the constant $P(H_2O)$, ΔV increased with $P(S_2)$, which can be regarded as caused by the increase of $P(S_2)$ or $C(H_2S)$. There is no previous study in which the effect of $C(H_2S)$ on fuel electrodes is separated from that of $P(S_2)$ to identify the dominant factor of sulfur-poisoning. ΔV was, therefore, measured with constant $C(H_2S)$ in order to separate the influence of $C(H_2S)$. The open circles indicate plots with constant $C(H_2S)$. The values of $C(H_2S)$ in the constant $C(H_2S)$ conditions at 1023, 1173 and 1273 K were

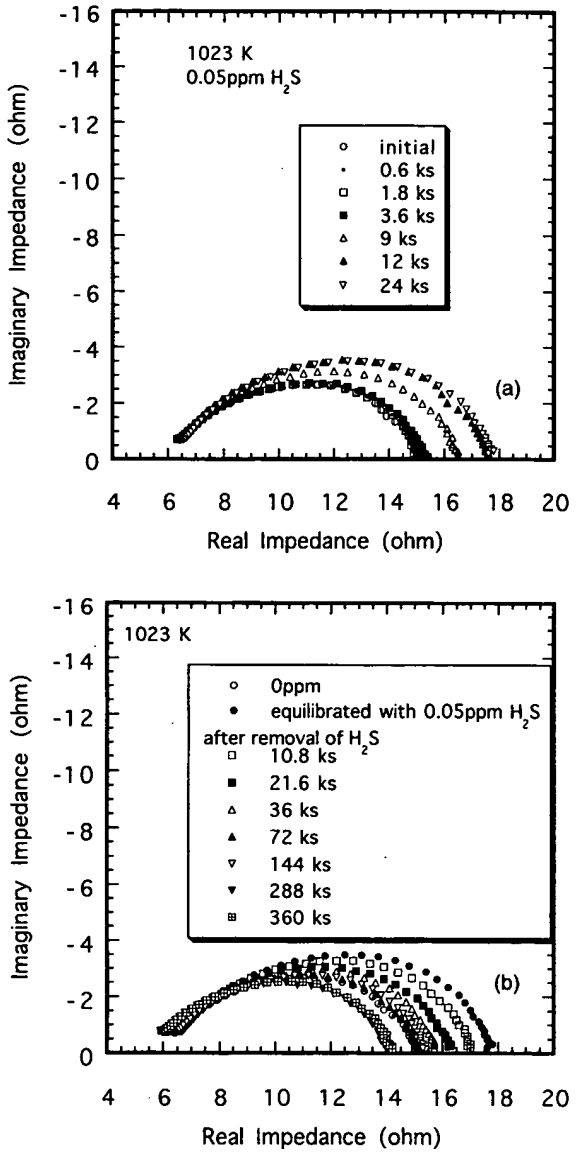

Fig. 8. The typical impedance spectra measured at 1023 K after (a) addition and (b) removal of 0.05 ppm H_2S.

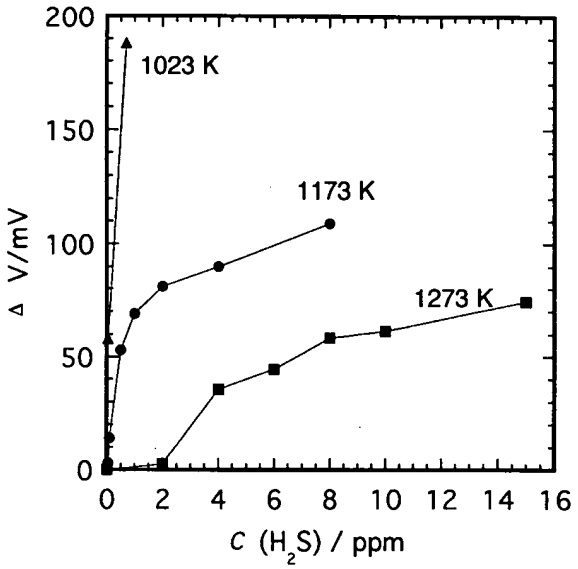

Fig. 9. The difference between the steady-state overvoltage in the fuel with H_2S and the initial overvoltage in the H_2S-free fuel as a function of $C(H_2S)$ at the current density of 0.3 A cm^{-2}.

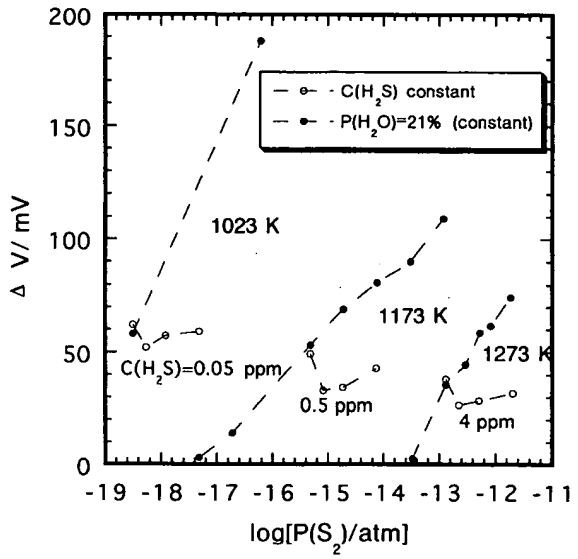

Fig. 10. The increase of the overvoltage as a function of $P(S_2)$; the open and closed circles indicate plots with constant $C(H_2S)$ and with constant $P(H_2O)$, respectively. The values of the constant $C(H_2S)$ are 0.05, 0.5 and 4 ppm for 1023, 1173 and 1273 K, respectively, and the value of the constant $P(H_2O)$ is 21% at all temperatures.

0.05, 0.5 and 4 ppm, respectively. It can be seen that the $P(S_2)$ dependence of ΔV in the fuel with constant $C(H_2S)$ is different from that in the fuel with constant $P(H_2O)$ at all temperatures. With the constant $C(H_2S)$, ΔV showed little dependence on $P(S_2)$. These results indicate that a factor dominating the poisoning by the sulfide impurity is not $P(S_2)$ but the total sulfur content in the fuel. In order to obtain

further information for investigation of the mechanism of the poisoning, an equivalent circuit analysis of the impedance spectra has been conducted [16].

4. Conclusions

The influence of the sulfide impurity on the electrochemical properties of the fuel electrode was investigated by using the complex impedance analysis and the DC polarization method. The polarization impedance and the DC overvoltage of the electrode increased when H_2S concentration exceeded 0.05, 0.5, and 2 ppm at 1023, 1173 and 1273 K, respectively. The time needed for the influence of the sulfide impurity to saturate was almost independent of the sulfide concentration, and was found to be about 12, 9 and 4 ks at 1023, 1173 and 1273 K, respectively. Within the experimental conditions, the performance loss caused by the sulfur-poisoning was recoverable when H_2S was removed from the fuel; the time needed for the recovery was found to be 360, 90 and 4 ks at 1023, 1173 and 1273 K, respectively. Thus, the poisoning effect has been found to have a large dependence on the operating temperature, which insists that a high-grade desulfurization will be necessary for reducing the operating temperature. From the dependence of sulfur poisoning on the equilibrium partial pressure of S_2 we have reached the conclusion that the sulfide poisoning was governed by the total sulfur content in the fuel.

References

[1] H.Y. Tu, Y. Takeda, N. Imanishi, O. Yamamoto, Solid State Ionics 117 (1999) 277.
[2] N.Q. Minh, J. Am. Ceram. Soc. 76 (1993) 563.
[3] S. De Souza, S.J. Visco, L.C. De Jonghe, Solid State Ionics 98 (1997) 57.
[4] J.W. Kim, A.V Virkar, K.Z. Fung, K. Mehta, S.C. Singhal, J. Electrochem. Soc. 146 (1999) 69.
[5] K. Ogasawara, I. Yasuda, Y. Matsuzaki, T. Ogiwara, M. Hishinuma, in: U. Stimming, S.C. Singhal, H. Tagawa, W. Lennert (Eds.), Proceedings of the 5th International Symposium on Solid Oxide Fuel Cells (SOFC-V), The Electrochemical Society Proceedings Series, Vol. PV 97-40, The Electrochemical Society, Pennington, NJ, 1997, p. 143.
[6] T. Ishihara, H. Matsuda, M. Azmi, Y. Takita, Solid State Ionics 86–88 (1995) 197.
[7] K. Huang, R.S. Tichy, J.B. Goodenough, C. Milliken, J. Am. Ceram. Soc. 81 (1998) 2581.
[8] R. Maric, S. Ohara, T. Fukui, H. Yoshida, M. Nishimura, T. Inagaki et al., J. Electrochem. Soc. 146 (1999) 2006.
[9] N.Q. Minh, T. Takahashi, in: Science and Technology of Ceramic Fuel Cells, Elsevier, Amsterdam, 1995, pp. 209–210.
[10] J. Geyer, H. Kohlmuller, H. Landes, R. Stubner, in: U. Stimming, S.C. Singhal, H. Tagawa, W. Lennert (Eds.), Proceedings of the 5th International Symposium on Solid Oxide Fuel Cells (SOFC-V), The Electrochemical Society Proceedings Series, Vol. PV 97-40, The Electrochemical Society, Pennington, NJ, 1997, p. 585.
[11] S.C. Singhal, R.J. Ruka, J.E. Bauerle, C.J. Spengler, Anode Development for Solid Oxide Fuel Cells, Report No. DOE/MC/22046-237 I, US Department of Energy, Washington, DC, 1986.
[12] D. Stolfen, R. Spah, R. Schamm, in: U. Stimming, S.C. Singhal, H. Tagawa, W. Lennert (Eds.), Proceedings of the 5th International Symposium on Solid Oxide Fuel Cells (SOFC-V), The Electrochemical Society Proceedings Series, Vol. PV 97-40, The Electrochemical Society, Pennington, NJ, 1997, p. 88.
[13] P. Primdahl, in: S.C. Singhal, M. Dokiya (Eds.), Proceedings of the 6th International Symposium on Solid Oxide Fuel Cells (sofc–vi), The Electrochemical Society Proceedings Series, Vol. PV 99-19, The Electrochemical Society, Pennington, NJ, 1999, p. 530.
[14] D.W. Dees, U. Balachandran, S.E. Dorris, J.J. Heiberger, C.C. McPheeter, J.J. Picciolo, in: S.C. Singhal (Ed.), Proceedings of the 1st International Symposium on Solid Oxide Fuel Cells (SOFC-I), The Electrochemical Society Proceedings Series, Vol. PV 89-11, The Electrochemical Society, Pennington, NJ, 1989, p. 317.
[15] M. Y Matsuzaki, T. Hishinuma, I. Kawashima, T. Yasuda, T. Koyama, in: Program and Abstracts of 1992 Fuel Cell Seminar, 1992, p. 119.
[16] Y Matsuzaki, I. Yasuda, Solid State Ionics (to be submitted).

(1960); DENT, A. L., AND KOKES, R. J., *J. Phys. Chem.* 73, 3772 (1969).
3. DENT, A. L., AND KOKES, R. J., *J. Amer. Chem. Soc.* 92, 6709 (1970); *J. Phys. Chem.* 74, 3653 (1970).
4. NIHIRA, H., FUKUSHIMA, T., TANAKA, K., AND OZAKI, A., *J. Catal.* 23, 281 (1971); TANAKA, K., AND BLYHOLDER, G., *J. Phys. Chem.* 76, 1394 (1972).
5. e.g., KRYLOV, O. V., "Catalysis by Nonmetals," p. 169. Academic Press, New York, 1970.
6. SAZONOV, B. A., POPOVSKII, V. V., AND BORESKOV, G. K., *Kinet. Katal.* 9, 312 (1968).
7. MORO-OKA, Y., AND OZAKI, A., *J. Catal.* 5, 116 (1966).

JOURNAL OF CATALYSIS 31, 173–199 (1973)

Activity of Nickel Catalysts for Steam Reforming of Hydrocarbons

JENS R. ROSTRUP-NIELSEN

Haldor Topsøe A/S, P.O. Box 49, DK-2860 Søborg, Denmark

Received March 7, 1973

A number of catalysts have been investigated to identify some factors of chemical composition and surface structure which may influence the activity for steam reforming of hydrocarbons. The kinetics for ethane reforming at 500°C are influenced by the composition of the catalyst. The specific activity is very low on some support materials, and when alkali is present. The activity correlates with the surface heterogeneity expressed by adsorption of nitrogen on the nickel surface. The activity trend observed for reforming of ethane is generally following that obtained for reforming of other hydrocarbons, hydrogenolysis of ethane, and methanation of carbon monoxide; whereas decomposition of ammonia appears unaffected by the carrier or the presence of alkali. Various explanations for the effect of the carrier and of alkali are discussed.

In many kinetic studies of chemical processes a single catalyst sample is investigated in great detail to provide a basis for calculation of the catalyst volume required for a given conversion in industrial reactors. Tubular steam reforming of higher hydrocarbons is a process where secondary effects of catalyst activity may have an influence comparable to that on the overall conversion. Steam reforming of higher hydrocarbons is a complex process including several consecutive and parallel reactions of which some may result in coke. The overall reaction can be described by the breakdown of the hydrocarbon:

$$C_nH_m + nH_2O \rightarrow nCO + \left(n + \frac{m}{2}\right) H_2 \quad (1)$$

followed by establishment of the equilibria:

$$CO + H_2O = CO_2 + H_2, \quad (2)$$

$$CO + 3H_2 = CH_4 + H_2O. \quad (3)$$

Tubular reformers are working normally at catalyst inlet and exit temperatures in the ranges 450–550 and 650–850°C, respectively. The catalyst activity determines the minimum exit temperature to be applied without breakthrough of higher hydrocarbons. This may be a problem in reformers for towns gas production (*1*, *2*). In most reformers for production of synthesis gas and hydrogen, the composition of the exit gas will be very close to the equilibria of reactions (2) and (3) established at the exit temperature and, normally, design restrictions to ensure long tube lives will determine the maximum throughput.

High catalyst activity may result in lower tube wall temperatures. In addition, it may imply reduced risks of coking because the breakdown of the higher hydrocarbons may be completed in the colder part of the bed where coking rates are smaller (*1*, *3*). However, this study deals only with the activity for conversion of the higher hydrocarbons, reaction (1), whereas the selectivity problems will be reported later. Moreover, the rates of the simultaneous reactions, (2) and (3), have not been considered and no attempts have been made to evaluate a complete kinetic expression to be applied in reactor design. As shown in Table 1 very different results have been reported on the kinetics of reaction (1) (*4–8*). Balashova, Slovokhotova and Balandin (*4*) observed the reaction order with

TABLE 1
RESULTS FROM SOME KINETIC STUDIES OF STEAM REFORMING OF HIGHER HYDROCARBONS

Authors	Catalyst system	Hydrocarbon	Temp (°C)	Pressure (atm abs)	Kinetic coefficients $\alpha_{C_nH_m}$	Kinetic coefficients α_{H_2O}	Activation energy (kcal/mol)
Balashova, Slovokhotova and Balandin (*4*)	Ni/SiO_2 Ni/C	Cyclohexane	400–460	(1)	0	0–1	22–24
					No activity		
Bhatta and Dixon (*5*)	Ni/γ-Al_2O_3	*n*-Butane	425–475	30	0	1	
Bhatta and Dixon (*6*)	Ni/γ-Al_2O_3	*n*-Butane		30	0	1	13
	Ni/α-$Al_2O_3UO_2$ (0.3% *K*)		404–491	30	1	−0.6	24
Phillips, Mulhall and Turner (*7*)	Ni/γ-Al_2O_3	*n*-Hexane *n*-Heptane	360–450	15	0.3	0–0.07	21
Saito *et al.* (*8*)	Ni/SiO_2	*n*-Butane	370–450	1	0	1	

respect to steam to vary with the range of steam partial pressure, and the data of Bhatta and Dixon (*6*) demonstrated that the kinetics may change significantly from catalyst to catalyst.

The purpose of the present work has been to identify some of the factors in chemical composition and surface structure of the catalyst which may influence the activity. Various catalyst preparations have been investigated but a more detailed kinetic study has only been made with a single catalyst sample. The study has been limited to temperatures around 500°C, a typical inlet temperature of the catalyst bed, because a high activity for reaction (*1*) is assumed to be important in this part of the bed. The activity has been estimated mainly from isothermal steam reforming experiments at atmospheric pressure. Ethane, being the simplest higher hydrocarbon, was selected as feed. Some experiments have been performed at pressure using various pure hydrocarbons and naphtha as feed. Finally, the activities for other reactions, methane reforming, methanation, decomposition of ammonia and ethane hydrogenolysis, have been estimated for some of the catalysts from experiments at atmospheric pressure. The activity tests have been supplemented by chemisorption studies.

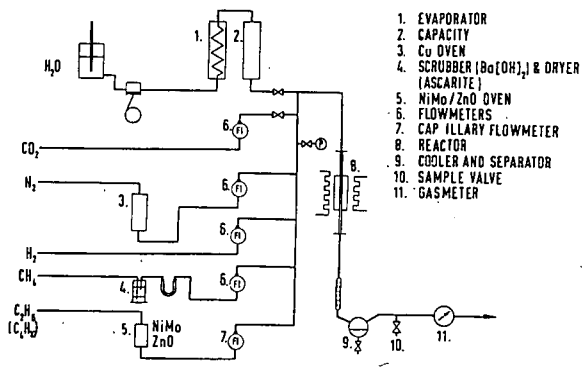

FIG 1. Apparatus for studies of ethane reforming and other reactions at atmospheric pressure.

METHODS

1. *Ethane Reforming at Atmospheric Pressure*

Apparatus. The experiments were performed in a simple flow system with a tubular fixed bed reactor as shown in Fig. 1. The reactor, which was made of 18/8 stainless steel, was surrounded by an electrically heated furnace. A metal block with an external diameter of 25 mm was mounted on the reactor to ensure isothermal conditions. The internal diameter of the reactor was 5.04 mm, and a thermowell with external diameter of 2.0 mm was placed in the axis of the reactor. The temperature of the catalyst bed was adjusted by means of a thyristor controller. The axial temperature gradient is estimated to be less than 1°C/cm in the catalyst bed.

The gas flows were controlled by flowmeters, whereas the addition of H_2O was followed on a buret.

Gases. All gases except H_2 were taken from cylinders. H_2 (impurities (mainly O_2) less than 0.03%) was made in an Oerlikon electrolyzer and used without further purification. C_2H_6 was purified over NiMo catalyst and ZnO at 270°C. Gas chromatographic analyses showed impurities of CH_4 (max 0.01 vol %), C_2H_4 (0.04–0.66 vol %), C_3H_8 (0.02–0.08), and C_3H_6 (0.02–0.40 vol %). N_2 was purified over Cu wire at 250–275°C. CO_2 was used without purification.

Procedure. A sample of 0.1–0.4 g of reduced catalyst as 0.3–0.5 mm particles was placed in the reactor. The catalyst was heated in H_2 (0.18 mol/hr) to the temperature to be used for the experiment (normally 500°C) and steam was added. After condensate was observed in the cooler and steam flow checked by sampling of condensate, ethane and, in a few experiments, also CO_2 were added. All experiments were performed with H_2 in the feed (H_2O/H_2 = approx 10) to avoid oxidation of the catalyst. When the exit gas flow was stabilized a sample of the dry exit gas was taken, and the conditions were changed. Normally, the activity stabilized within less than 30 min. However, over periods of days a gradual deactivation was observed which could be ascribed to sulfur poisoning. Owing to this the bed was changed after each run, normally having a maximum duration of approx 6 hr. In a few cases the bed was used for two runs. The parameter to be changed during the run was varied unsystematically with time to minimize the influence of poisoning. Moreover, as a check each experiment was completed at the same conditions as the starting conditions. After each experiment the weight of the catalyst was checked.

The gas sample was analyzed by means of Orsat (CO_2) and gas chromatographic analysis. At the normal conditions the main products were CO_2 and H_2.

Evaluation. The reaction of ethane with steam:

$$C_2H_6 + 4H_2O = 2CO_2 + 7H_2, \qquad (4)$$

can be considered irreversible as K_p (500°C) = 155 atm^4.

For simplicity a kinetic expression of the power form was selected:

$$r = F\frac{dx}{dw} = Ae^{-E_a/RT}\prod_i p_i^{\alpha_i}, \qquad (5)$$

where $F = C_2H_6$ inlet flow, W = catalyst weight, and x = conversion. The conversion of C_2H_6 was calculated on basis of the exit gas analysis by:

$$x = \frac{(CH_4) + (CO) + (CO_2)}{(CH_4) + (CO) + (CO_2) + 2(C_2H_6)} \times 100\%. \qquad (6)$$

The kinetic parameters were estimated from plots of the conversion and the parameter in question, and the estimated values were used for computer integrations of (*5*) assuming no diffusion restrictions and no temperature gradients. On the basis of the calculated rate constants the kinetic parameters were changed until the variance was minimized. In the calculations the measured H_2O addition was used as the H_2O-feed, whereas the inlet gas flows were calculated on the basis of the exit gas analysis and the measurement of the exit gas flow. This procedure was found to be more accurate than using the readings of the flowmeters. The mass balance of the apparatus was checked in a few experiments where gas samples were taken before and after the reactor. Relative deviations in ethane contents of less than 1% were indicated. Blank experiments at 500°C with alumina particles showed no conversion.

The calculation procedure described could not be applied in experiments with C_2H_6 and CO_2 in the feed, and in all these experiments gas samples were taken before and after the reactor. The inlet gas flows of CO_2 and C_2H_6 were calculated from the CO_2/C_2H_6 ratio of the feedgas, the exit gas analysis and the exit flow. The conversion was calculated from the ethane mass balance.

In order to compare the activities of catalysts with different kinetic parameters the initial rate r_i was calculated at following standard conditions: $H_2O/C_2H_6 = 8$; $H_2O/H_2 = 10$; temperature = 500°C; and pressure = 1.0 atm abs.

2. *Other Reactions Tested at Atmospheric Pressure*

The apparatus used for ethane reforming experiments was also used for experiments on methane reforming, ammonia decomposition, and ethane hydrogenolysis. CH_4 and NH_3 were taken from cylinders. CH_4 containing less than 0.02% of higher hydrocarbons was purified by washing in a $Ba(OH)_2$ solution and over ascarite to remove an impurity of CO_2 (0.7 vol %). NH_3 was used unpurified.

The methane reforming experiments were evaluated in a similar way as the ethane reforming experiments assuming first order kinetics with respect to methane as generally agreed in the literature (*9, 10*):

$$r = k \cdot p_{CH_4}(1 - Q/K_p), \qquad (7)$$

where Q and K_p are reaction quotient and equilibrium constant for:

$$CH_4 + 2H_2O = CO_2 + 4H_2. \qquad (8)$$

The activities were compared by the initial rates calculated at the same standard conditions as above with $H_2O/CH_4 = 4$.

In the experiments on decomposition of ammonia:

$$2NH_3 = N_2 + 3H_2, \qquad (9)$$

the unconverted ammonia was absorbed in a solution of sulfuric acid and the conversion was calculated from the amount of washed exit gas and the ammonia feed. The activity was expressed as the conversion at 500°C using a space velocity of 9.0 mol NH_3/g cat/hr.

The experiments on ethane hydrogenolysis:

$$C_2H_6 + H_2 = 2CH_4, \qquad (10)$$

were performed with following feed:

C_2H_6	5 vol%
H_2	20 vol%
N_2	75 vol%.

Reaction (10) is generally reported to be first order with respect to C_2H_6 (*11*), whereas the order with respect to H_2 may vary. However, the partial pressure of H_2 can be considered as constant due to the large excess and the conversions being less than 10%. Therefore, the activity was expressed as the first order rate constant at 300°C.

The methanation experiments were performed in the apparatus used and described by Schoubye (*12*). A mixture of H_2 containing approx 1 vol % CO was used as feed (0.1 Nm^3/hr). The reaction:

$$CO + 3H_2 = CH_4 + H_2O, \qquad (11)$$

was performed isothermally at a temperature in the range 200–300°C depending on the expected activity. The catalyst was used as 0.4–0.5 mm particles in amounts of 0.5 g. The initial rate was calculated on the basis of the kinetics of Schoubye (*12*) at the following standard conditions: 1 vol % CO in H_2; temperature = 250°C; pressure = 1.0 atm abs.

3. *Reforming Experiments at Elevated Pressure*

Apparatus. The apparatus was designed to simulate operation under industrial conditions. Water and liquid hydrocarbon feed were pumped to an evaporator and mixed with gaseous hydrocarbons and N_2 to be used as feed. The feed mixture was passed through a vessel for mixing and a preheater to a tubular reactor. H_2 was added just before the reactor. The reactor effluent was depressurized and passed through a cooler and a separator to a gas meter.

The reactor was made of 18/8 stainless steel and had an internal and external diameter of 10.0 and 17.5 mm, respectively. One thermowell with external diameter 3 mm was placed in the axis of the reactor, and another at the external surface. The reactor was surrounded by an electrically heated furnace with 3 independent sections. The heated length of the reactor was 60 cm, whereas the height of the catalyst bed was 10 cm. The catalyst zone consisted of 0.25—approx 10 g of catalyst as 1–2 mm particles diluted to constant volume with particles of magnesium aluminum spinel. The amount of catalyst was determined such that conversions and temperature gradients were of the same order of size in all experiments. Above the catalyst zone was placed a layer of 5 cm of particles of magnesium aluminum spinel. The temperature was adjusted by thyristor controllers, and the pressure was maintained by a pneumatic control valve. The flows of water and liquid hydrocarbons were indicated on burets, whereas the gas feeds were measured on flowmeters. The axial temperature gradient in the catalyst bed was found to be approx 1°C/cm, whereas the temperature difference between the external tube wall and the axis of the bed varied between 2 and 10°C. On this basis the experiments cannot be considered as strictly isothermal, and the results may only be used for relative comparisons of the catalysts.

Feedstock. The compositions of the feedstocks were determined by gas chromatographic analysis. The liquid hydrocarbons were desulfurized in a separate apparatus over NiMo catalyst and ZnO. Analyses showed contents less than 0.05 ppm S. The gaseous hydrocarbons, N_2 and H_2 were used unpurified.

Procedure. Before each experiment the apparatus was checked for leakages in H_2 at 36 atm abs. The reactor was heated up in H_2 to about 400°C. Steam and then gradually hydrocarbon feed were added and the process conditions were established. All experiments were performed with addition of H_2, ($H_2O/H_2 = 10$), to avoid oxidation. It soon turned out that the catalyst activity could not be maintained for more than a few hours. This could be ascribed to sulfur poisoning caused by the quick accumulation of sulfur at the extremely high throughputs. Therefore, most of the experiments included only one measurement. As standard conditions were used:

Pressure	31 atm abs
Mean temp	500°C
H_2O/C	4 mol/atom
H_2O/H_2	10 mol/atom

In a few experiments where the total pressure was changed, this was done in an unsystematic way to minimize the influence of poisoning. Samples of dry exit gas and in some cases a sample of unconverted hydrocarbon were taken and analyzed by means of a gas chromatograph and Orsat analysis (CO_2).

Evaluation. The conversion, x, of the higher hydrocarbons was calculated from the analysis and flow measurement of the exit gas giving the g atoms of CO, CO_2 and CH_4 formed, and from the measured consumption of liquid hydrocarbon giving the total g atoms of C in the feed. In the experiments with gaseous feed the conversion was calculated on basis of the exit gas only. Assuming pseudo-first order kinetics with respect to the hydrocarbon an apparent constant k_a was calculated from:

$$k_a = \frac{F}{W} \ln\left(\frac{1}{1 - x}\right). \qquad (12)$$

In an experiment with CH_4 as feed, x was replaced by x/x_{eq} where x_{eq} is the conversion to establish the equilibrium. As described by Hougen and Watson (*13*) for situations where the kinetic expression is unknown, it may be useful for comparing different catalysts to assume that even complex catalytic systems approximate to a pseudo-first order relationship if only space velocity is varied. However, it must be emphasized that the apparent rate constant obtained by this empirical method may hardly be used for prediction of catalyst performance at other conditions. It should be used only for relative comparison

TABLE 2
PROPERTIES OF CATALYSTS: A-TYPES

Catalyst no.	Comments	Na (wt %)	Contents of red. Ni (wt %)	Ni area (m^2/g)	Total area (BET) (m^2/g)	n_0 N_2-capacity (B_5) (N cm^3/kg)	Particle size: Calc. r_{mean} (Å)	Particle size: Electron microscope particle ϕ (Å)	Activity for C_2H_6 reforming 500°C: r_i (mol/g/hr × 10)	Activity for C_2H_6 reforming 500°C: r_s (mol/m^2 Ni/hr × 10^3)
Group 1. Fixed composition (25 wt % Ni). Na: 0.04–0.16 wt %. Preparation route 1.										
A1		0.07	23.8	2.00	20.0	14	398	250–2500	2.4	120
A15		0.04	22.0	3.01		34	245		4.40	145
A3		0.05	16.4	6.97	45.5	172	79	50–250	8.25	118
A4		0.05	23.1	3.78	33.3	5	205	500–1000	2.0	53
A16		0.14	22.9	2.99			257		1.5	52
A7	A16 sintered	0.16	23.5	1.06			740	150–2000	0.51	48
A17		0.10	26.4	2.72		80	326		1.4	52
A18		0.08	25.7	3.46	27.4	50	249		4.2	122
Group 2. Fixed composition (25 wt % Ni). Na < 0.01 wt %. Various preparation routes.										
A19	A1 washed in H_2O					108			4.0	198
A20	Preparation route 2		18.1	3.71	15.7	112	163		8.2	222
A21	A20 sintered		10.1	1.09	2.34		311		2.0	183
A22	Preparation route 1		20.0	4.16	25.1	79	161		11.9	287
A23	A22 sintered		22.9	1.08	8.6	5	684		2.9	282
A24	Preparation route 1		20.4	8.87	53.7		77		20.4	230
A25	Preparation route 3		20.3	6.34	39.8	179	107		10.5	165
Group 3. Ni content varied. Na < 0.01 wt %. Preparation route 1.										
A10	Ni/Mg = 1/1	0.04	13.9	4.17		96	112	50–125	10.6	254
A26	0.25/1		4.3	2.12			68	75–200	1.9	90
A27	0.5/1		8.2	4.35			63	75–200	9.5	212
A28	1/1		14.2	6.10			78	75–200	18.4	299
A29	2/1		23.9	8.50			94	75–300	16.8	197
A30	4/1		35.1	8.45			139	200–600	18.6	221
A31	6/1		41.9	3.64			385	500–1000	8.0	219
A32	8/1		48.3	3.35			485	2000–5000	7.1	214
Group 4. Other metals (total content of metals 25 wt %) Na < 0.01 wt %. Preparation route 1.										
A13	Ni/Cu = 0.7/1.3		7.6	(1.23)				50–150	0.020	1.6
A14	Ni replaced by Co		22.9[a]	5.48			140	(500)	0.016	0.29
A33	Ni/Co = 3/1		25.0[a]	6.34			132		2.9	46
Group 5. Promoted with alkali (25 wt % Ni)										
A34	A1 0.14 wt % K[b]			2.95					0.79	27
A35	A1 0.53 wt % K[b]			2.65					0.097	3.7
A36	A25 2.1 wt % K[c]			3.58	43.5	70	107		0.075	2.1
A37	A1 0.61 wt % Na[b]			2.44					0.32	13
A38	A24 0.11 wt % Na[b]								13.4	151
A39	A24 0.46 wt % Na[b]								7.2	81
A40	A24 0.78 wt % Na[b]								7.6	86

[a] Red. Co or Co + Ni.
[b] Alkali added after reduction.
[c] Alkali added during preparation.

TABLE 3

PROPERTIES OF CATALYSTS: B–E TYPES

Catalyst type	Support material	Comments	Contents of red. Ni (wt %)	Ni area (m^2/g)	Total area (BET) (m^2/g)	n_0 N_2 capacity (B_5) (ml/kg)	Particle size: Calc r_{mean} (Å)	Particle size: Electron microscope particle ϕ (Å)	Activity for C_2H_6 reforming 500°C: r_i (mol/g/hr × 10)	Activity for C_2H_6 reforming 500°C: r_s (mol/m^2 Ni/hr × 10^3)
Type B. Based on $MgAl_2O_4$										
B1	$MgAl_2O_4$		8.0	0.44	4.19	12	607	500–2500	1.6	366
B5	$MgAl_2O_4$	1.57 wt % K[a]	11.1	1.35			272		0.029	2.1
B6	$MgAl_2O_4$	0.52 wt % K[a]	17.0						0.54	61
B4	$MgAl_2O_4$	1.53 wt % K[a]	17.5	0.88			664		0.074	8.3
Type C. Based on Al_2O_3										
C1	η-Al_2O_3		16.5	7.01		65	79	100–400	5.5	80
C6	η-Al_2O_3 Cl	1.7 wt % K[b]		6.34		29			1.8	29
C7	η-Al_2O_3 Cl	5.8 wt % K[b]		3.89		0.5			0.45	11
C8	η-Al_2O_3 Cl	1.3 wt % Na[b]		6.78		13			3.2	47
C9	η-Al_2O_3 Cl	1.1 wt % Ca[b]		7.24		115			2.2	30
C2	γ-Al_2O_3		17.9	5.66	106	238	106		9.2	163
C3	γ-Al_2O_3		20	3.62	71.1	196	185		8.2	227
C10	γ-Al_2O_3 C3	2.1 wt % K[a]		4.19	76.4	13	160		1.9	46
C4	γ-Al_2O_3	red. at 500°C	44.3	11.31		586	131		34.3	304
C5	α-Al_2O_3		6.3	1.39			121		2.0	141
Type D. Based on various materials										
D2	MgO		5.3	1.61			146		4.3	266
D3	MgO, Al_2O_3, ($MgAl_2O_4$) Mg/Al = 0.5		19.1	14.5			44		17.4	120
D4	ZrO_2		16.2	2.58		0.5	210		0.067	2.6
D5	ZrO_2/γ-Al_2O_3	Zr/Al = 0.44	25.0	5.70			147		11.5	201
D6	Cr_2O_3	red. at 500°C	60.0	7.92			254		19.9	252
D8	SiO_2		21.2	12.67	145		53		16.8	133
D9	SiO_2/Al_2O_3	Si/Al = 3	21.2	4.43		382	76		1.1	25
D10	SiO_2/Al_2O_3	Si/Al = 2.1 3.9% Na[a]	25	2.45	44		336		0.44	18
D11	SiO_2/MgO	Si/Mg = 1.67	25	2.42	33		346		0.58	24
D12	D11 with 0.49 wt % K[a]		25	2.13	10		394		0.097	4.5
D13	TiO_2		37.0	1.00			125		0.36	36
D14	Carbon[c]		14.4	(0.8)				500–1700	0.040	5
D7	Cr_2O_3	red. at 500°C	12.3	5.43			76		14.1	260
Type E. Containing precious metals										
E1	Al_2O_3	Pt	0.5[e]	0.24[e]					0.53	221
E2	Al_2O_3	Pt	5.0	1.54					1.2	77
E3	carbon[d]	Pt	0.5	0.55						
E4	Al_2O_3	Pd	0.5	0.41					0.87	212
E5	Al_2O_3	Pd	5.0	3.46					6.7	180
E6	γ-Al_2O_3	Pd		0.10					0.19	194
E7	carbon	Pd	0.5	0.20						
E8	Al_2O_3	Ru	0.5	0.26					5.4	2059
E9	Al_2O_3	Ru	5.0	1.81					30.3	1673
E10	γ-Al_2O_3	Ru		0.55					0.20	37
E11	carbon[d]	Ru	0.5	0.48						
E12	γ-Al_2O_3	Rh		0.17					4.1	2502
E13	carbon[d]	Rh	0.5	0.37						
E14	γ-Al_2O_3	Re		0.21					0.10	50

[a] Added during preparation.
[b] Added before reduction.
[c] Ni area estimated from particle diameter.
[d] Diluted with γ-Al_2O_3, 1/10.
[e] Following figures based on metals indicated.

of catalyst activities or reactivities of various hydrocarbons.

4. Catalysts

The catalysts which are listed in Tables 2 and 3 have been divided into various types determined by their chemical compositions. The A-type is based on magnesia containing approx 6 wt % Al. Group 1 has a minor content of Na (0.02–0.16 wt %) whereas groups 2–4 are free of alkali metals (less than 0.01 wt %). Group 2 includes catalysts with fixed composition but with different preparation routes whereas the Ni content is varied in group 3. The B-type is based on magnesium aluminum spinel whereas the C-type is supported by various types of alumina. Catalysts based on other supports are represented by Type D and, finally, type E covers catalysts containing precious metals. If not indicated in the tables the catalysts of groups B–E contain no alkali metals (less than 0.01 wt %). The numbering of the catalysts is made in accordance with the numbering used previously (*14*). Some of the catalysts were prepared in parallel and may present a better basis for comparisons. In addition to what is indicated in Tables 2 and 3 such groups are (A20–A23), (A26–A32), (B1 and B4–B6), and (A25, A36, C7, C8, D8, D10 and D11).

The catalysts were reduced in a separate reactor at 850°C in H_2 for a period of 2 hr unless otherwise indicated. The content of nickel in the reduced state was determined as previously (*14*). The nickel surface area was calculated on basis of the sulfur capacity assuming the saturated surface to contain 44.2×10^{-9} g S/cm². The sulfur capacity was determined by chemisorption of H_2S at 500°C as described previously (*15*). A mean particle radius was calculated from the nickel surface area and the content of reduced nickel as shown earlier (*14*). This figure should be used only as an indication. For some catalysts the range of nickel particle size was estimated by means of an electron microscope. A N_2 capacity of the Ni surface was determined by a procedure described below.

5. Adsorption Studies

The presence of special sites on the nickel surface was investigated on basis of the work by Van Hardeveld *et al.* (*16–19*) who found that N_2 was physisorbed on the so-called B_5-sites of nickel crystallites in the range 15–70 Å in a polarized state which was infrared active. The polarization explains the relatively high initial heat of adsorption (approx 13 kcal/mol). Other studies (*20–22*) have considered the IR active N_2 as weakly chemisorbed molecules, whereas the results of Bradshaw and Pritchard (*23, 24*) appear consistent with those of Van Hardeveld *et al.*

As demonstrated by Van Hardeveld and Van Montfort (*19*) the determination of the number of B_5-sites either by IR or volumetric methods is not unambiguous, as there is no simple correlation between the intensity of the IR-absorption band of the adsorbed N_2 and the number of B_5-sites. The results make it likely that all N_2 adsorbed at room temperature and relatively low pressure is adsorbed in the IR-active form, but this N_2 is only a fraction of that which can be adsorbed at higher pressure or lower temperature. On this basis Van Hardeveld (*25*) has proposed measurement of the adsorbed volume at room temperature and a N_2 pressure of 200 mm Hg as a standard method for determination of the number of B_5-sites.

This method has been adopted here, and as a correction for ordinary physically adsorbed N_2, the measurement was repeated after poisoning the nickel surface with N_2O. The N_2 capacity, n_0, was determined as the difference between the two adsorbed volumes at 200 mm Hg. The measurements were performed in a conventional BET apparatus as described previously (*15*). A sample of 15–20 g of prereduced catalyst was heated in a flow of H_2 and evacuated for approx 3 hr at 800°C to a pressure below 10^{-4} mm Hg before the measurements. The high evacuation temperature was necessary to remove all H_2 from the surface. It was evident that H_2 could still be removed when heating the evacuated sample from 600 to 800°C. Evacuation at 600°C only resulted in smaller values of the N_2 capacity. Catalyst C4 was reduced in the equipment at 500°C but evacuated at 800°C.

Some isotherms are shown in Fig. 2. For catalyst C4, which was the catalyst with the highest N_2 capacity, the contribution from the physically adsorbed N_2 is negligible, whereas the N_2 capacity of a typical catalyst like A1 is determined as the difference between two figures of same order. This makes the determination of n_0 very uncertain. Even catalyst C4 shows a value of n_0 of approximately one order of magnitude less than the typical values of the catalyst of Van Hardeveld. This is explained by the larger nickel crystallites of the present catalysts. The high uncertainty of the small adsorption volumes makes an estimation of the initial heat of adsorption very unsafe. On basis of the isotherms on C4 at 25 and 65°C an initial isosteric heat of adsorption was estimated to about 11 kcal/mol N_2.

Results

1. Ethane Reforming

A series of experiments was performed to determine a kinetic expression for ethane reforming at 500°C over catalyst A1. Minimum variance for an expression of the form (5) was obtained by:

$$r = 1.67 \times 10^5 e^{-18100/RT} p_{C_2H_6}{}^{0.54} p_{H_2O}{}^{-0.33} p_{H_2}{}^{0.2} \text{ mol/g} \cdot \text{hr}. \quad (13)$$

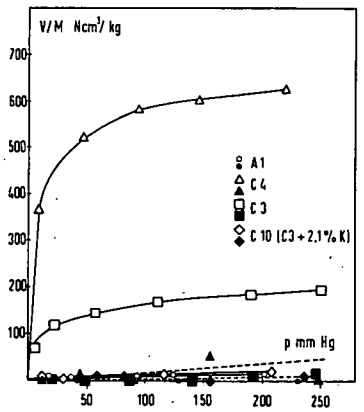

FIG. 2. Isotherms for N_2-adsorption at 25°C. Measurements after passivation of Ni surface with N_2O indicated by filled points and broken lines.

The effect of the partial pressure of carbon dioxide appeared insignificant. Experiments at 450 and 550°C including variations of the partial pressure of steam showed $\alpha_{H_2O} = -0.60$ and -0.23, indicating that a more complex expression is required to describe the kinetics of the reaction in a broad temperature range. In this connection it should be noticed that Bodrov, Apel'baum and Temkin (*9*) found the kinetic coefficient of hydrogen to vary with temperature in their studies of the methane reforming reaction.

The kinetic coefficients, mainly for steam, were determined for some other catalysts. As shown in Table 4 the reaction order with respect to steam varied significantly from catalyst to catalyst. Thus, catalysts containing free magnesia (A-types and D3) showed negative values of α_{H_2O} down to -0.5, whereas catalysts based on magnesium aluminum spinel (B1) or alumina (C1) showed values of zero or slightly positive, respectively. The addition of potassium caused a significant decrease of α_{H_2O}. The addition of sodium had a less pronounced effect. The addition of potassium implied no change of the apparent activation energy whereas replacement of nickel with a nickel–copper alloy caused a substantial increase of the activation energy. This is demonstrated in Fig. 3.

The influence on the experiments of mass and heat transfer was analyzed by means of the Topsøe REACTOR program (*26*) designed for computer calculation of the temperature and conversion profiles of a fixed bed converter. The calculation is performed on the basis of the intrinsic kinetics and the pore volume distribution of the catalyst. For catalyst A18, a catalyst at a typical activity level, the calculation showed an effectiveness factor of more than 0.95 and a temperature drop over the gas film surrounding the particles of 1.3°C, which reflects only negligible restrictions. For a very active catalyst such as A22,

TABLE 4
ETHANE REFORMING AT ATMOSPHERIC PRESSURE, 500°C: SUMMARY OF KINETIC PARAMETERS[f]

Catalyst type	Comments	Kinetic coefficients C_2H_6	H_2O	H_2	Apparent activation energy E_a, (kcal/mol)	
Type A, Group 1 (MgO)						
A1		0.54[a]	−0.33[a]	0.2[a]	18.1	(0.15)
A18			−0.52[b]			
	Group 2					
A19			0.0			
A21			−0.26[c]			
A22			−0.48[c]			
A23			−0.17[c]			
A13					24.4	(0.7)
	Group 5 (Promoted)					
A34	A1, 0.14 wt % K		−0.42[c]		18.9	(0.3)
A35	A1, 0.53 wt % K		−1.81[e]		19.6	(0.5)
A37	A1, 0.61 wt % Na		−0.7			
Type B, ($MgAl_2O_4$)						
B1			0.0[b]		18.3	(2.5)
B4	1.53 wt % K	(0.4)[c]	−1.08[d]			
Type C, (Al_2O_3)						
C1		(0.6)[c]	0.13[a]			
Type D						
D3	MgO/Al_2O_3 = 1/1		−0.26[b]			
D4	ZrO_2				19.2	(0.9)

[f] Figures in brackets indicate the accuracies of the activation energies. The accuracies of the coefficients are estimated to: [a] ≤0.05; [b] 0.05–0.1; [c] 0.1–0.2; [d] 0.2–0.3; [e] 0.3–0.5.

some transport restrictions were indicated by an effectiveness factor of approx 0.9 and a temperature drop over the gas film of 4–5°C.

Due to the variations in kinetic coefficients from catalyst to catalyst the activities were compared on the basis of initial rates r_i as described previously. For catalysts for which no kinetic coefficients were determined, r_i was calculated on the basis of the kinetics of a similar catalyst. The relative standard deviations of r_i calculated from experiments based on samples of the same origin and of the corresponding nickel areas were estimated to be approx 17 and 10%, respectively, which yield a relative standard deviation of the specific rate r_s of no better than 20%. Therefore, the experiments only allow identification of substantial differences of specific activity.

From the results shown in Tables 2 and 3 the alkali-free nickel catalysts appear to have a specific activity in the range r_s = 0.1–0.35 mol/m² Ni/hr. This is observed on a broad range of support materials such as magnesia in various sintered forms, and with Al/Mg ratios varying from 0 to 2, magnesium aluminum spinel, alumina in different modifications, alumina stabilized by zirconia, chromia and silica. Moreover, results from a systematic series of catalysts (A22–A32) shown in Fig. 4 indicate only insignificant influence on the specific activity of the nickel content and of the nickel crystallite size varying with the nickel content from 50 to 5000 Å. The results might reflect less specific activity on the smallest crystallites but more experiments with catalysts with nickel crystallites below 70 Å are required to elucidate this effect.

Some alkali-free catalysts show a small specific activity. The catalysts based on silica–alumina, silica–magnesia and on titania had r_s = 0.02–0.04 mol/m² Ni/g, whereas the activity of catalysts based on pure zirconia and carbon was very poor with $r_s = 2.6 \times 10^{-3}$ and 3.8×10^{-4}, respectively. The low activity of the zirconia based catalyst (D4) is not accompanied by an activation energy differing from that of catalyst A1. The activity of the zirconia–alumina based catalyst (D5) appears normal, which may be explained by nickel being supported mainly by alumina as it was present as nickel aluminum spinel before the reduction.

The addition of potassium to the catalysts can result in a decrease of the specific activity of more than one order of magnitude. This is demonstrated in Fig. 5 which indicated the influence to be stronger on A- and B-types than on C-types. The effect of sodium addition is less than that of potassium. The significant influence of potassium is remarkable as sulfur poisoning of catalyst A1 involving a gradual blocking of the nickel surface is causing a decline of the specific activity by only approx 50%. This appears from Table 5 showing in addition an influence of other poisons such as chlorine and arsenic being less than that of potassium.

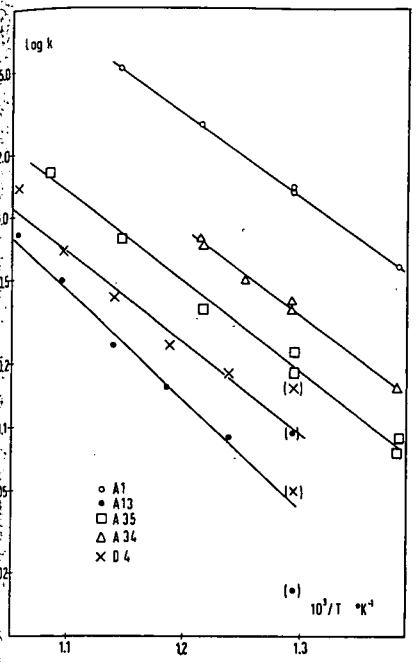

FIG. 3. Temperature dependence of rate constant for ethane reforming at 500°C.

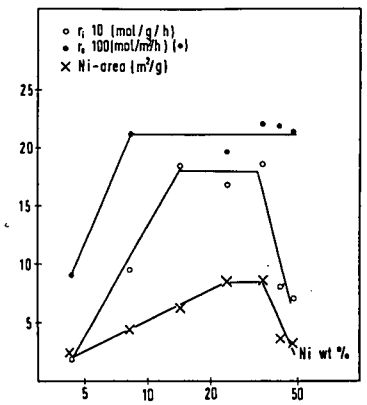

FIG. 4. Influence of Ni content on Ni surface area and activity for ethane reforming at 500°C. Catalysts A26–A32.

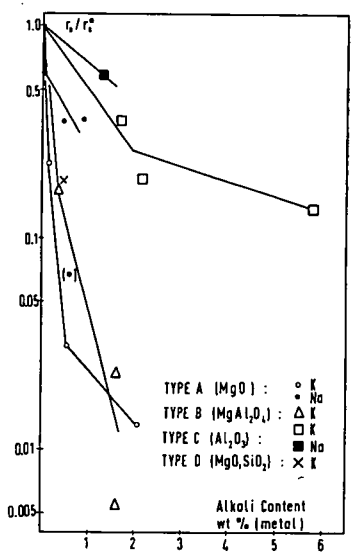

FIG. 5. Influence of alkali on the specific activity for ethane reforming at 500°C.

TABLE 5
THE INFLUENCE OF POISONS ON THE ACTIVITY OF CATALYST A1

Expt no.	Poison	Content (wt ppm)	Sulfur capacity (wt ppm)	Coverage	$r_i \times 10$ (g mol/g/hr)	$r_s \times 10$ (g mol/m² Ni/hr)
Av of unpoisoned A1	—	80	883	<0.1	2.41	120
4201	S	239	805	0.30	0.66	62
4202	S	360	805	0.45	0.53	69
4203	S	398	805	0.49	0.59	64
329	S	615	805	0.76	0.38	56
55	S	805	805	1.00	<0.01	—
133	Cl	1350	885	?	2.43	
141	As	4200	885	?	0.55	

The presence of potassium implied no decrease of the nickel surface area determined by chemisorption of hydrogen sulfide at 550°C or as demonstrated previously (*15*) by chemisorption of hydrogen at −72°C. However, the measurements of nitrogen adsorption on the nickel surface shown in Tables 2 and 3 were significantly influenced by the addition of potassium. As, moreover, the nitrogen capacity of the zirconia-based catalyst D4 was negligible, it is natural to correlate catalyst activity and nitrogen capacity. This has been done in Fig. 6 and a correlation coefficient of 0.94 indicating great significance was calculated. Although the correlation reflects the great uncertainty of the adsorption measurements and does not account for the relatively low activity of the silica–alumina supported catalyst D9, it seems likely that the differences in specific activities are related to inhomogeneities of the nickel surface. It does not necessarily ascribe a special high activity to B_5-sites, as the number of these sites in some way is correlated with the number of other surface configurations such as corner atoms with low coordination numbers.

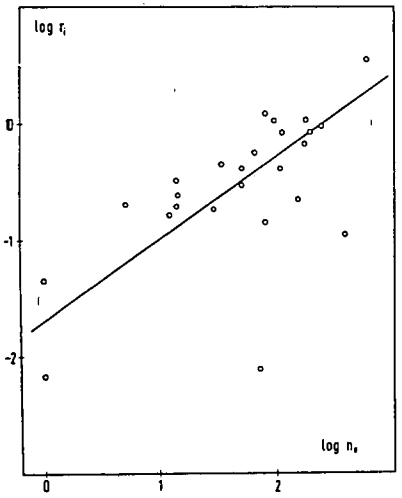

FIG. 6. N_2 capacity and activity for ethane reforming at 500°C.

Measurements on catalysts containing different metals showed large variations of specific activities. From Tables 2 and 3 the specific activities of metals based on alumina or magnesia may be listed as follows:

$$Rh, Ru > Ni, Pd, Pt, > Re > (Ni_{0.7}Cu_{1.3}) > Co.$$

The low activity of E10 could be explained by some irregularities in the preparation. The low activity of cobalt may be related to the process conditions with a H_2O/H_2 ratio close to the equilibrium constant for oxidation of cobalt by steam. The precious metals supported by carbon showed very poor activities similar to the results with carbon supported nickel catalysts.

2. *Other Reactions at Atmospheric Pressure*

In some reforming experiments with catalyst A1, ethane was replaced by methane or *n*-butane. First order kinetics were applied for methane reforming experiments. This was justified by an experiment showing the kinetic coefficient to be close to unity. Equation (13) was used for evaluation of butane reforming experiments. The results are summarized in Table 6. The initial specific rates have been calculated at the same partial pressure of the hydrocarbon. The apparent activation energy is higher for methane than for ethane reforming, and a smaller reactivity is reflected by a lower initial specific rate. Contrary to this *n*-butane shows an activation energy and molar specific rate very close to that of ethane. This implies that the rate per carbon atom is higher for *n*-butane than for ethane. Moreover, it was observed that in the temperature range 400–525°C the reaction with *n*-butane resulted in no higher hydrocarbons among the products.

TABLE 6
REFORMING EXPERIMENTS AT ATMOSPHERIC PRESSURE VARIOUS HYDROCARBONS, CATALYST A1

Feed	Sp act (500°C)[a] × 10³ r_s (mol/m² hr)	Sp act (500°C)[a] × 10³ r_{sc} (g atom/m² hr)	App. activation energy[b] E_a (kcal/mol)
CH_4	61	61	26.2 (0.4)
C_2H_6	120	240	18.1 (0.15)
nC_4H_{10}	138	552	18.6 (0.6)

[a] Rates calculated for same partial pressure of hydrocarbon ($H_2O/C_nH_m = 8$; $H_2O/H_2 = 10$; 500°C).

[b] Figures in parentheses indicate the accuracy of E_a.

Results from experiments on hydrogenolysis of ethane and decomposition of ammonia are shown in Figs. 7 and 8, respectively. The trends of activities for these reactions, methane reforming and methanation of carbon monoxide were compared with the activity trend for ethane reforming by calculating activities relative to catalyst A1. The results are shown in Table 7.

The activity trends for ethane and methane reforming, ethane hydrogenolysis and methanation are broadly in line. Thus, the presence of potassium affects all these reactions by decreasing the specific activity. The data for methanation show some deviations from those for ethane reforming. Firstly, the catalysts based on zirconia (D4) and carbon (D14) show relatively high activities. Secondly, it appears that the specific activity of highly active catalysts, particularly those based on alumina, is higher than the corresponding values for ethane reforming. On the other hand, the influence of alkali appears to be more pronounced for methanation.

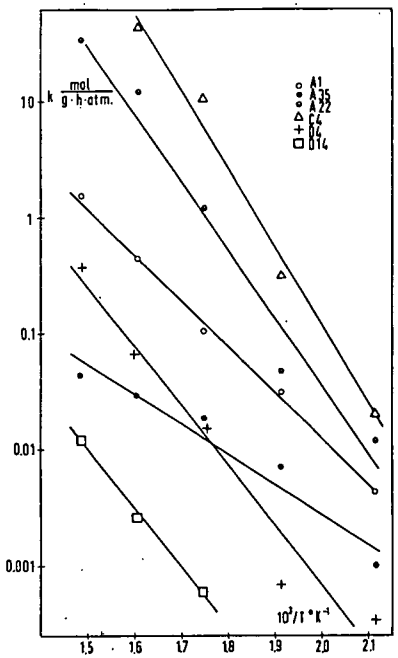

FIG. 7. Ethane hydrogenolysis. Temperature dependence of rate constants for various catalysts.

The results from decomposition of ammonia differ significantly from the general trend, as no decrease of the specific activity is observed for potassium-promoted catalysts and D4. No large changes of specific activities are observed, and as shown in Fig. 9 the activities for ammonia decomposition correlate simply with the nickel area. The cobalt-containing catalyst (A33) fits into this correlation.

3. *Reforming Experiments at Pressure*

The reforming experiments at pressure with 1–2 mm particles were subject to great

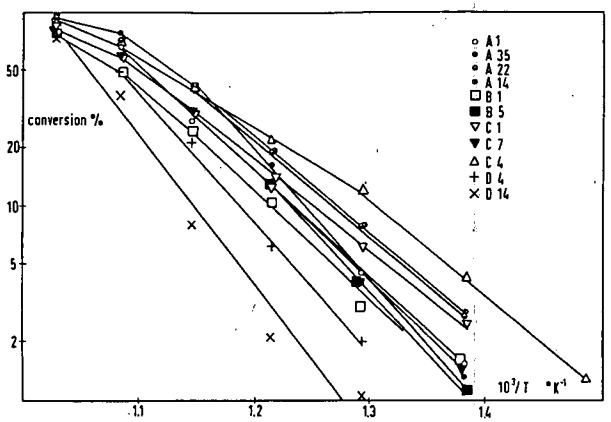

FIG. 8. Ammonia decomposition. Temperature dependence of conversion at standard conditions.

uncertainty as explained previously. This makes a more detailed evaluation doubtful. However, the results plotted in Fig. 10 show the conversion of ethane to increase with pressure. In principle, this could be explained by Knudsen diffusion causing severe restrictions at low pressure but the results from the experiment, 1231, performed at constant pressure and varying nitrogen flow indicates the pressure effect on the conversion to be related to the kinetics. When using naphtha as feed, positive and negative pressure effects are observed depending on the type of catalyst. As shown in Fig. 11 the conversion increases with pressure for catalysts A1 and B6, whereas the opposite effect is observed for the strongly alkalized B4. These results correlate with the kinetic coefficients for ethane reforming at atmospheric pressure listed in Table 4 which indicates the overall pressure coefficient to be positive for A1 and B6 and negative for B4.

The activities of various catalysts obtained by reforming of naphtha at 31 atm abs correlate with the corresponding activities determined by ethane reforming at atmospheric pressure. This is demonstrated in Fig. 12, where the straight line reflects the correlation for equal specific activities.

TABLE 7
RELATIVE SPECIFIC ACTIVITIES AT ATMOSPHERIC PRESSURE

Catalyst		Reforming		Hydrogenolysis of	Methanation of	Decomp. of
No.	Remarks	C_2H_6 500°C	CH_4 500°C	C_2H_6 300°C	CO 250°C	NH_3 500°C
A1	(0.07 wt % Na)	1.0	1.0	1.0	1.0	1.0
A22		2.4	2.0	4.2	9.1	0.9
A35	0.53% K	0.03	0.09	0.08	0.002	0.9
B1		3.0	1.4			3.2
B5	1.57% K	0.02	0.02			1.5
C1		0.7			2.7	0.4
C4		2.5		8.7	20.6	0.5
C7	5.8 wt % K	0.09			0.001	0.5
D4	ZrO_2	0.02	0.01	0.08	0.8	0.4
D8	SiO_2	1.1			4.9	
D9	SiO_2/Al_2O_3	0.2			0.04	
D14	Carbon	0.04	0.04	0.01	0.4	0.5

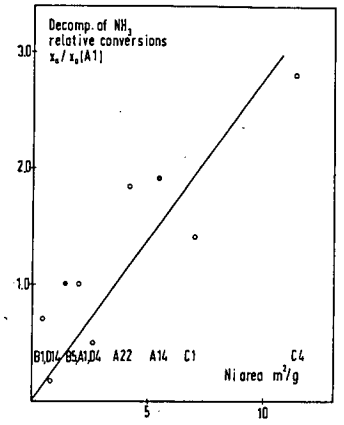

FIG. 9. Ammonia decomposition at 500°C. Activity as function of nickel surface area. Activity expressed as conversion at standard conditions relative to catalyst A1.

Experiments with various hydrocarbons performed at 31 atm abs and 500°C using a fixed steam to carbon ratio revealed great differences in conversions. As shown in Table 8 most hydrocarbons are more reactive than is methane. Normal paraffins appear less reactive than isoparaffins and naphthenes whereas the reactivity of benzene is very close to that of methane. However, it should be noticed that the experiments are performed at a fixed steam to carbon ratio which implies that the partial pressure of the hydrocarbons varies with the number of carbon atoms of the hydrocarbon. As mentioned previously, extrapolation by means of the apparent rate constant k_a is very doubtful. When the con-

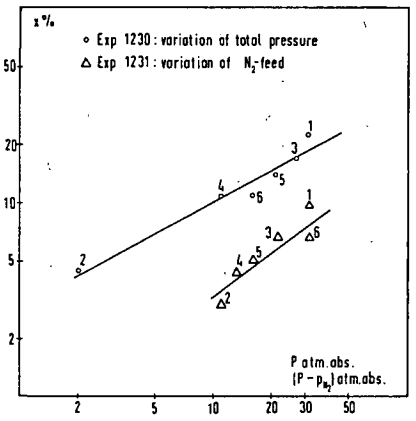

FIG. 10. Ethane reforming at pressure. Pressure dependence of conversion at standard conditions at 500°C. 0.5 g catalyst A18. The numbers indicate the sequence of measurements.

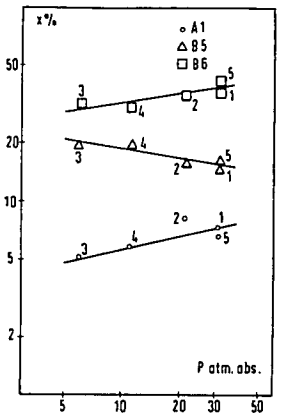

FIG. 11. Reforming of naphtha 36 at pressure. Pressure dependence of conversion at standard conditions at 500°C. Expt 1206: 0.5 g A1; Expt 1195: 10.7 g B5 (1.5 wt % K); Expt 1196: 11.7 g B6 (0.3 wt % K). Numbers indicate sequence of measurements.

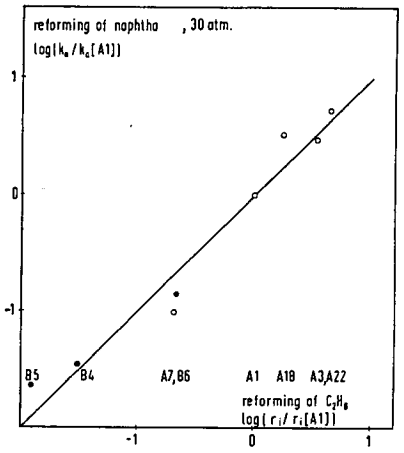

FIG. 12. Correlation between relative activities at 500°C for reforming of naphtha 36 at 30 atm and reforming of ethane at atmospheric pressure. Activities expressed relative to catalyst A1.

TABLE 8
REFORMING AT PRESSURE[a]

Exp. no.	Feed	H_2O/C (mol/atom)	$p_{C_nH_m}$ (atm)	Space velocity $\frac{\text{g atoms} \cdot 22.4}{\text{kg cat.}} \times 10^3$	Conversion to CO, CO_2, CH_4 (%)	k_a calc. from (13) (g atom/g/hr)	$k_a \times$ (no. C-atoms/ no. C-C bonds)	$k_a \times \frac{p_{CH_4}}{p_{C_nH_m}}$
1211	Methane	3.71	6.0	194	4.65[b]	0.43	—	0.43
1212	Ethane	3.79	3,3	207	31.5	3.5	1.8	6.4
1230		3.85	3.2	204	22.5	2.3	1.2	4.3
1216	(*n,iso*)Butane)	3.85	1.7	204	39.9	4.6	3.5	16
1210	Cyclohexane	3.73	1.2	209	53.9	7.2	7.2	36
1208	Benzene	3.96	1.1	200	5.7	0.53	0.53	2.9
1209	*n*-Heptane	3.83	1.0	206	18.7	1.9	1.6	11
1214	Trimethyl-butane	3.88	1.0	201	33.2	3.6	3.1	22
1213	*n*-Decane	3.77	0.7	104	32.8	1.9	1.7	16
1203	Naphtha 36 (FBP 120°C)	3.74	—	209	40.0	4.8	—	—
1215		3.76	—	209	35.8	4.1	—	—
1207	Naphtha 49 (FBP 169°C)	3.69	—	212	15.5	1.6	—	—

[a] Experiments with various hydrocarbons; Catalyst A18 (0.5 g as 1-2 mm particles); temp. 500°C; pressure 31 atm abs; $H_2O/H_2 = 10$.
[b] Conversion to CO and CO_2.

stants are corrected for the actual partial pressures of the hydrocarbons and assuming first order kinetics as shown in Table 8, the results indicate normal paraffins to be more reactive with increasing number of carbon atoms. This trend is still obtained when assuming a reaction order of 0.5 with respect to the hydrocarbon, and it is in accordance with the results obtained at low pressure shown in Table 5.

The analyses of higher hydrocarbons in the reactor effluent shown in Table 9 indicate the composition to be very close to that of the feedstock. This observation is in accordance with the result obtained in the reforming experiment with *n*-butane at atmospheric pressure. Therefore, the presence of intermediates in the products is very unlikely. The experiment with benzene represents an exception to this picture, and a detailed evaluation of the analysis of the unconverted naphtha from experiment 1207 appears very complicated.

DISCUSSION

1. *Kinetics*

Although the kinetics of ethane reforming appear complex it may be helpful to discuss qualitatively the parameters involved in terms of a simple speculative sequence. Ethane is assumed to be chemisorbed on nickel following the pattern generally proposed in studies of ethane hydrogenolysis (*11*). An initial chemisorption step on a dual site involving dehydrogenation is followed by a rupture of the carbon–carbon bond and formation of a surface radical CH_x. Adsorption of steam on the carrier is assumed to be involved on the basis of the observed influence on the kinetic coefficient for water of the type of support material and of the presence of alkali. A rôle of the carrier for steam adsorption has also been suggested in the literature (*4, 6, 8*). When S_1 and S_2 are empty sites on the surface of nickel and the carrier respectively, the following sequence can be formulated:

$$C_2H_6 + 2S_1 = (S_1)_2\text{–}C_2H_z + \frac{6-z}{2}H_2, \quad (14)$$

$$(S_1)_2\text{–}C_2H_z + H_2 = 2S_1\text{–}CH_x, \quad (15)$$

$$H_2O + S_2 = S_2\text{–}H_2O, \quad (16)$$

$$S_2\text{–}H_2O + S_1 = S_1\text{–}O + H_2S_2, \quad (17)$$

$$S_1\text{–}CH_x + S_1\text{–}O = 2S_1 + CO + \frac{x}{2}H_2, \quad (18)$$

$$CO + S_1\text{–}O = S_1 + CO_2. \quad (19)$$

Certainly, steps (14) and (15) represent a simplification because there may be a gradual formation of strongly adsorbed species by further dehydrogenation. As discussed by Kemball (*27*) and Frennet and Lienard (*28*) these species may become less reactive and may therefore diminish the surface available for the reaction. Eventually they may be converted to carbon.

For ethane hydrogenolysis the rupture of the carbon–carbon bond is generally assumed to be the rate determining step of the overall reaction, all other steps being in quasi-equilibrium (*11, 29, 30*). In other studies (*31–33*) it is believed that the desorption of products is rate determining. Recently Boudart (*34*) has considered the reaction as two irreversible steps.

These opposite views are reflected by the assumptions made in the formulation of kinetics for reforming reactions. Balashova, Slovokhotova and Balandin (*4*) argued for the rupture of the carbon–carbon bond as the rate determining step, whereas Bhatta and Dixon (*5*) and Saito *et al.* (*8*) were in favor of the desorption of products or the reaction with steam being the slow step. Phillips, Mulhall and Turner (*7*) suggested that the rate determining step varies with the type of hydrocarbon, whereas Bodrov, Apel'baum and Temkin (*9*) for methane reforming assumed the reaction with steam to be rate determining at low temperature and the chemisorption of methane to be limiting at high temperature.

There are some objections to discussing the kinetics by means of a single rate determining step. Firstly, as proposed by Boudart (*34*), the dissociative chemisorption of ethane is most probably irreversible in the temperature range of the present study. Secondly, for practical purposes, the surface reaction (18) might also be considered as irreversible since no influence on the

TABLE 9
REFORMING EXPERIMENTS WITH VARIOUS HYDROCARBONS[a]

Expt no.:	1216 Butane		1210 Cyclohexane		1208 Benzene		1209 *n*-Heptane		1214	1213	1215 1203	1207 Naphtha 49[d]	
Feed: Analyses (wt %)	Feed[b]	Liq. prod.[c]	Feed	Liq. prod.	Feed	Liq. prod.	Feed	Liq. prod.	Tri meth. buta. Feed	*n*-Decane Feed	Naphtha 36[d] Feed	Feed	Liq. prod.
C_2H_4	0.01	0.04											
C_2H_6	0.05	0.47										0.10	
$C_3H_8 + (C_3H_6)$	1.20	1.57										1.13	
n-C_4	80.30	79.00									0.02	3.70	
i-C_4	17.92	18.61										1.08	
C_4H_8	0.27	0.00							0.05				
n-C_5	0.25	0.31			0.01	0.01	0.06	0.02	0.32		29.16	3.92	2.05
i-C_5							0.01		0.11		8.55	4.45	0.22
CP											1.74	0.51	0.22
n-C_6				1.65	0.01	0.08	0.82	0.57			16.51	4.39	4.51
i-C_6				0.02		0.04	0.06	0.04			16.84	4.70	3.58
MCP(+22DMP)				0.92	0.04	0.03	0.17	0.10			3.40	2.72	1.20
CH(+33DMP)			99.98	96.34	0.07	0.06	0.47	0.36	0.06		1.86	1.80	1.19
Benzene					99.71	62.23	0.05	0.24	0.56		1.24	0.23	0.39
n-C_7			0.01	0.72	0.02	0.38	86.40	87.71	0.01		5.14	5.21	7.02
iso-C_7				0.18	0.07	0.17	8.45	7.67	98.78		5.45	4.78	5.50
DMCP				0.01		0.11	1.72	1.52			1.53	4.31	3.06
MCH(+22DMH + 113TMCP)			0.01	0.06		0.35	0.72	0.69			1.72	6.66	5.49
ECP(+25DMH)				0.01		0.11	0.19	0.18			0.52	1.04	1.15
Toluene				0.03		0.38	0.37	0.36			1.76	1.82	2.70
n-C_8						3.26	0.31	0.35			1.02	6.40	7.16
iso-$C_8 + C_{8+}$				0.06	0.07	3.30	0.20	0.19			2.33	11.87	14.60
ECH						0.82					0.09	2.53	1.74
Ethylbenz						0.54					0.12	0.30	1.10
Xylenes						3.00					0.33	4.36	4.48
n-C_9						5.06					0.37	4.60	5.02
C_{9+}						10.26					0.17	10.43	15.41
n-C_{10}						1.61				>95	0.06	0.18	1.43
C_{10+}						7.02					0.07	2.07	9.62
n-C_{11}						0.09							0.06
C_{11+}						1.09							1.10

[a] Temp: 500°C; pressure: 30 atm abs; catalyst: A18; gas chromatographical analyses of feed and liquid products.
[b] CH_4: 0.01 vol %.
[c] Calculated from gas analysis.

[d] Naphtha no.:	36			49		
ASTM: IBP/MBP/FBP (°C)	40	65	120	40	89	169
Spec gr (g/ml)	0.674			0.705		

rate of carbon dioxide was indicated. Moreover, the surface species S_1–CH_x and probably also S_1–O may be assumed to be the most abundant surface intermediates, the concentrations of other intermediates being negligible. There is some evidence for this assumption. As no intermediates are found in the products when using *n*-butane or higher hydrocarbons (except benzene) as feed, this may indicate the same active species, containing one carbon atom, to be involved in the reaction. In addition, some LEED studies by Maire *et al.* (*35*, *36*) have shown similar structures of the type CH_x to be formed by adsorption on nickel of methane, ethane, propane and neopentane.

These assumptions lead to the following equations for the rates of the steps and for the total number of sites, L and M, on the surface of nickel and carrier, respectively:

$$r_{14} = r_{15} = \tfrac{1}{2}r_{18} \quad r_{+16} = r_{-16} \quad r_{+17} = r_{-17},$$

$$(S_1) + (S_1\text{–}CH_x) + (S_1\text{–}O) = L,$$

$$(S_2) + (S_2\text{–}H_2O) = M, \quad (20)$$

the remaining steps involved in establishment of the equilibria (2) and (3) being kinetically insignificant in accordance with the principle formulated by Boudart (*34*). Using Langmuir equations and thus assuming a homogeneous surface and no changes of heats of adsorption with coverage the following rate equation is obtained:

$$r = \frac{k_A L^2 \cdot p_{C_2H_6}}{[(1 + (2k_A/k_r)\,(1/K_w)(p_{C_2H_6}/p_{H_2O})p_{H_2} + K_w(p_{H_2O}/p_{H_2})]^2}, \quad (21)$$

where $k_A = k_{14}$, $k_r = k_{18}$ and $k_w = k_{+16} \cdot k_{+17}/(k_{-16} \cdot k_{-17})$.

From this expression it is possible qualitatively to comprehend the varying kinetic coefficients reported in the literature (Table 1) and observed in this study (Table 4). The kinetic order with respect to steam may become positive or negative depending on the size of the equilibrium constant for steam adsorption, K_w, and the relative sizes of the rate constants for the hydrocarbon adsorption, k_A, and the surface reaction, k_r. Since K_w is the product of the equilibrium constants of steps (16) and (17) it is strongly influenced by the adsorption properties of the carrier material. A possible temperature dependence of reaction orders is clear since the relative size of the terms of denominator may change with temperature depending on the sizes of the activation energies for the hydrocarbon adsorption and the surface reaction, and the heat of adsorption for steam. The different reactivities of various hydrocarbons may be reflected by the size of k_A, which may also be affected by the presence of some optimal sites on the nickel surface. Surface heterogeneities were ignored in the derivation of (21) but as demonstrated by Boudart (*34*, *37*) this will still lead to rate functions being qualitatively correct. If step (15) is assumed to be rate determining the second term of the denominator in (21) disappears. An expression of that form was derived by Lička (*38*).

Equation (21) may be converted to a power–rate law using the well-known approximation of the term $ax/(1 + ax)$ by the term bx^α where $0 < \alpha < 1$:

$$r = k_n p_{C_2H_6}{}^{1-2m} \cdot p_{H_2O}{}^{2(n-m)} p_{H_2}{}^{2(m-n)}, \quad (22)$$

where $0 < m < 1$, and $0 < n < 1$.

This expression may explain the kinetic coefficients obtained for catalyst A1 as shown in (13), and that the kinetic coefficient for steam may become less than -1 as observed for catalysts A35 and B4, but the reaction orders with respect to steam and hydrogen are not numerically equal as predicted.

In addition, the overall pressure coefficients to be deduced from Fig. 11 correlate with the kinetic order for steam indicating the rôle of hydrogen to be more complicated than accounted for in the simple sequence.

In Boudart's (*34*) recent kinetic interpretation of ethane hydrogenolysis hydrogen is assumed to be in a chemisorption equilibrium with nearby saturated sites on the metal surface different from the sites where the hydrocarbon reacts. If so, step (14) should be reformulated by:

$$H_2 + 2S_3 = 2(S_3)\text{–}H, \quad (23)$$

$$C_2H_6 + 2S_1 + yS_3 = (S_1)_2\text{–}C_2H_x + y(S_3)\text{–}H + \frac{6 - y - z}{2}H_2. \quad (24)$$

This implies that the term $p_{C_2H_6}$ in (21) and (22) should be replaced by $p_{C_2H_6}/p_{H_2}{}^{y/2}$. Hence:

$$r = \frac{k'_A(p_{C_2H_6}/p_{H_2}{}^{y/2})}{[1 + (2k'_A/k_r)(1/K_w) \cdot (p_{C_2H_6}/p_{H_2O}) \cdot p_{H_2}{}^{1-(y/2)} + K_w(p_{H_2O}/p_{H_2})]^2}, \quad (25)$$

$$r = kp_{C_2H_6}{}^{1-2n} \cdot p_{H_2O}{}^{2(n-m)} \cdot p_{H_2}{}^{2(m-n)-(n/2)y}. \quad (26)$$

The simple sequence for hydrocarbon adsorption simulating the steps suggested in hydrogenolysis remains speculative, and it may hardly be used for evaluation of the reactivity trend of the higher hydrocarbons because the results from hydrogenolysis have been reported mainly for temperatures below 400°C.

The apparent multiple fission of carbon–carbon bonds and the relatively high reactivity of branched hydrocarbons and cyclohexane deviates from the pattern generally observed in hydrogenolysis at low temperature, nickel attacking selectively the ends of chains (*39*). However, in reforming studies in the temperature range 250–350°C Balashova, Slovokhotova and Balandin (*40*) found a stepwise degradation of hydrocarbons and a much higher reactivity of *n*-paraffins than of cycloparaffins. At higher temperatures, 350–450°C, Phillips, Mulhall and Turner (*7*) observed partially decomposed hydrocarbons from the reforming reaction with branched hydrocarbons which were less reactive than normal paraffins. Methyl cyclohexane was found to be slightly less reactive than normal heptane and a small amount of toluene was found among the products. In the present study at 500°C intermediates were indicated only for benzene this being the least reactive hydrocarbon. In experiments at very high temperatures 750–950°C, Yoshitomi, Morita and Yamamoto (*41*) found cyclohexane to be more reactive than *n*-hexane above approx 800°C. Although thermal pyrolysis must have influenced the latter results, the relative reactivities appear to vary with temperature. This conclusion is supported by the different activation energies for normal and cycloparaffins reported by Balashova, Slovokhotova and Balandin (*40*).

At 600°C Schnell (*42*) was able to detect substantial amounts of low olefins in reforming experiments with propane and butane performed at very short contact times. In the present experiments on butane reforming at atmospheric pressure conversions and contact times (approx 2×10^{-3} sec) were within the range considered by Schnell. Since no intermediates were identified in these studies performed at 400–525°C, the olefins observed by Schnell are most probably not intermediates from the reaction on the nickel surface but products from thermal pyrolysis or cracking on the carrier material, these reactions being more pronounced at the temperature level applied by Schnell. On this basis, it appears reasonable to assume multiple fission of the carbon–carbon bonds on the nickel surface for most nonaromatic hydrocarbons at temperatures of 500°C and above, and to consider minor amounts of ethane, propane and other higher hydrocarbons which might be observed in the effluent of some tubular reformers as being hydrogenated products from pyrolysis or cracking.

2. *Catalyst Activity*

The results shown in Table 7 demonstrated that the specific activity of nickel for reforming reactions, hydrogenolysis and methanation is strongly influenced by the carrier employed and by the presence of alkali. A parallelism of activity trends is observed. Another common feature of these reactions is a resemblance of the trend of specific activities of different metals, ruthenium and rhodium being reported to show much higher specific activities for hydrogenolysis (*11*) and methana-

tion (*43*) than do nickel, platinum, and palladium. Contrary to this, ammonia decomposition appears unaffected by the carrier and the presence of alkali. This makes doubtful the use of this reaction for activity tests of reforming catalysts as proposed by Merkel (*44*).

A carrier effect in reforming reactions has also been described by Balashova, Slovokhotova and Balandin (*4*) who found nickel on carbon to be nearly inactive for reforming of cyclohexane compared with nickel on silica. Balashova, Slovokhotova and Balandin explained the difference by a failing ability of coke for activation of steam since the two catalysts showed comparable activities for dehydrogenation of cyclohexane. However, as proven by the hydrogenolysis experiments, nickel on carbon may show poor activity in other reactions where steam is not involved.

A low activity for hydrogenolysis has also been reported by Sinfelt (*11*) for cobalt on carbon. Moreover, Sinfelt showed the specific activity for hydrogenolysis of silica–alumina-based nickel catalysts to be much less than those of alumina- or silica-based catalysts, the latter being the most effective. These results are in accordance with the trend observed for ethane reforming in the present study, although the accuracy of the experiments does not allow a distinction between alumina- and silica-based catalysts. For methanation of carbon dioxide Pour (*45*) found the specific activity of supported nickel to decrease in the order chromia, alumina, silica.

The diminution of the activity for reforming reactions caused by alkali was mentioned by Andrew (*3*). The effect was explained by adsorption of alkali blocking the most active sites on the nickel surface. When this explanation is applied for the present measuements, it implies that the adsorption of alkali is not affecting the sites for ammonia decomposition. Moreover, it implies that alkali is adsorbed more specifically at the most active sites than is sulfur, because as mentioned earlier, the specific activity displays a more drastic fall by increasing the amount of alkali than by increasing the amount of sulfur. This behavior appears unlikely but, in principle, it cannot be excluded, as demonstrated by Roginskii (*46*).

The effect of alkali has also been reported for hydrogenolysis. Cimino, Boudart and Taylor (*47*) observed a great effect of alkali on the kinetics of ethane hydrogenolysis on iron. This effect was explained by assuming alkali to depress the affinity of the surface for hydrogen so that dehydrogenation of the adsorbed hydrocarbon is retarded. In the simple sequence (14) this means a higher value of z. Shephard (*33*) observed a similar effect on a nickel alumina catalyst and noticed that removal of alkali resulted in increased specific activity. For methanation of carbon monoxide Schoubye (*12*) reported low activities of alkali-promoted catalysts.

The evaluation of interactions between metal and support has been an intricate subject of catalysis. Bifunctional catalysis is not very likely to be involved apart from the rôle of the carrier in steam adsorption which cannot explain the different specific activities. As discussed earlier, cracking on the carrier surface may be excluded in the temperature range applied in the experiments and no correlation between surface acidity and specific activity is apparent. Thus catalysts based on magnesia, spinel and γ-alumina show specific activities within the same range. A similar conclusion on a rôle of acid sites for hydrogenolysis was arrived at by Richardson (*48*).

The electronic nature of the support was emphasized in the work by Schwab *et al.* (*49*) and Szabo and Solymosi (*50*). A change of the activation energy with the doping of oxides supporting thin nickel films was assigned to a change of the semiconductor properties of the carrier influencing the Fermi level of the electrons of the metal phase. However, from later developments (*51*) there is much evidence for the localized chemical properties of the surface atoms being important for the catalytic reaction rather than the collective properties of the bulk phase. Therefore, apart from extremely small metal crystallites as used by Dalla Betta and Boudart (*52*) an electronic interaction between the carrier and the surface atoms of the metal is very unlikely. The measurements reported in Table 4 and Fig. 3 are in accordance with this statement, as the use of zirconia (D4) or the presence of alkali (A34 and A35) resulting in low specific activities are accompanied by no detectable change of the activation energies. Contrary to this, an increased activation energy observed when using a nickel–copper catalyst (A13) may be explained by an influence on the nickel surface atoms of neighboring copper atoms.

As mentioned earlier the correlation shown in Fig. 6 indicates that different specific activities might be related to the heterogeneity of the nickel surface which presumably is influenced by the carrier. The reforming reactions, hydrogenolysis and methanation may therefore be characterized as structure-sensitive, while decomposition of ammonia appears "facile". The effect of surface structure is often studied on a series of catalysts with varying metal crystallite size because heterogeneity of the surface is expected to increase by decreasing the crystallite size in the range below approx 70 Å (*17*). In hydrogenolysis results appear ambiguous, as Sinfelt (*11*) found an effect for nickel on silica–alumina, whereas the activity showed no variation with crystallite size for nickel on silica. For methanation on nickel supported by alumina Bousquet and Teichner (*53*) found no influence on the specific activity of crystallite size. The nickel crystallites of the catalysts in the present study are nearly all outside the range of interest, and reforming of ethane appears to be unaffected by the crystallite size as shown in Fig. 4, although a decrease of the specific activity with crystallite size might be indicated for the catalyst with the smallest crystallites.

Meanwhile, surface heterogeneity is not only a result of crystallite size but rather a matter of surface topography, with the existence of ensembles of nickel atoms on the surface being optimal for the particular reaction in question. The configuration of such ensembles may vary from reaction to reaction. Thus, Ponec and Sachtler (*54*) from their work on nickel–copper alloys suggested that the ensembles required for reactions affecting the carbon–hydrogen bond or leading to isomerization contain a smaller number of adjacent nickel atoms than the ensembles required for hydrogenolytic splitting of the carbon–carbon bond.

On larger crystals the number of special ensembles may vary with crystal orientation (*55*, *56*) or the ensembles may be related to epitaxial relations or abnormal shapes of the crystals which could be stabilized by the support material. The interface is extremely complex as chemical reactions may be involved. In principle, the shape of the metal particle is influenced by the anisotropy of the surface energy of the metal and by the interfacial energy (*57*). Unfortunately, very few studies have been reported on this effect. For liquid nickel droplets at 1500°C Kingery (*58*, *59*) found a significantly higher adhesion energy and correspondingly low interfacial energy and contact angle for stabilized zirconia as support than for alumina. Studies *in vacuo* of nickel droplets on various materials indicated by low contact angles that wetting was more pronounced on graphite than on several oxides. Contact angles on zirconia and titania were lower than on magnesia, alumina and beryllia. Preferential adsorption of impurities at the interface may lower the interfacial energy and result in facetting and other equilibrated shapes (*58*, *60*, *61*).

It is evident that these observations allow no conclusions to be made concerning the effect of the carrier on the catalytic activity of the metal. In addition, use of data obtained for droplets at high temperature appears doubtful. However, there may be some indication that carrier materials showing high adhesion energy and thus influencing the shape of the metal particle cause a decrease of the number of ensembles for the reforming reactions. Moreover, it is conceivable that the influence of alkali is caused by adsorption of alkali at the interface or on the metal changing the shape of the crystal or the facetting of the planes. Shephard (*33*) also considered the importance of various crystallite forms for the activity for hydrogenolysis. Exami-

nation in the electron microscope of the catalysts of this study revealed no marked differences between active and poor catalysts, and more detailed studies on well-defined systems are required to evaluate these effects.

Conclusions

The kinetics and the specific activity for reforming reactions vary from catalyst to catalyst. The major differences in the kinetics are found in the influence of steam partial pressure. This is related to the ability of the carrier material to adsorb steam. Active magnesia or the presence of alkali enhance steam adsorption. The kinetics cannot be described in a broad temperature range by a simple power law, as the powers vary with temperature.

At temperatures around 500°C the results indicate multiple fission on the nickel surface of the carbon–carbon bonds for most nonaromatic hydrocarbons. The reactivity of normal paraffins at equal partial pressures appears to increase with the number of carbon atoms. The reactivity of branched hydrocarbons and cycloparaffins appear higher than those of normal paraffins whereas aromatics show poor reactivity.

The activities per unit nickel surface area, the specific activities, are within the same range for a great number of catalysts irrespective of the nickel surface area, support material, preparation or activation procedure. Use of supports such as zirconia and carbon results in very poor specific activities, whereas some decrease of the specific activity is observed when using silica–alumina and titania. Addition of alkali in various ways implies a significant drop in specific activity, the effect of potassium being larger than for sodium.

The activity trends observed for reforming reactions are generally in accordance with results obtained or reported for ethane hydrogenolysis and methanation, whereas the specific activity for decomposition of ammonia appears unaffected by the carrier and the presence of alkali. It is unlikely that this effect of the carrier and alkali is related to the ability for steam adsorption or to surface acidity. Morever, electronic interactions between carrier or alkali and the metal may be excluded, since the effect is not accompanied by a change of the activation energy.

The results indicate that the activity for reforming correlates with the surface heterogeneity as expressed by the adsorption of nitrogen on the nickel surface. It is believed that some carrier materials and adsorption of alkali on the interface or the metal may influence the surface structure by changes of the surface and interfacial energies. This might affect the number of ensembles being optimal for reforming reactions, hydrogenolysis and methanation.

Acknowledgments

The author thanks Dr. Haldor Topsøe for encouraging this work and his permission to publish the results. Thanks are given to Mrs. G. Parthum, Mr. J. Holst, Mr. C. Thomsen, Mr. P. Tøttrup, and many colleagues for assistance in performing the experiments. Mr. J. E. Jarvan has kindly assisted in preparing the computer calculations.

References

1. Rostrup-Nielsen, J. R., *Chem. Eng. Progr. Ammonia Safety Symp. Tech. Man.* 15, (1973) in press.
2. Bridger, G. W., and Wyrwas, W., *Chem. Proc. Eng.* 48, 101 (1967).
3. Andrew, S. P. S., *Ind. Eng. Chem., Prod. Res. Develop.* 8, 321 (1969).
4. Balashova, S. A., Slovokhotova, T. A., and Balandin, A. A., *Kinet. Katal.* 7, 303 (1966).
5. Bhatta, K. S. M., and Dixon, G. M., *Trans. Faraday Soc.* 63, 2217 (1967).
6. Bhatta, K. S. M., and Dixon, G. M., *Ind. Eng. Chem., Prod. Res. Develop.* 8, 324 (1969).
7. Phillips, T. R., Mulhall, J., and Turner, G. E., *J. Catal.* 15, 233 (1969).
8. Saito, M., Tokuno, M., Ichiro, A., and Morita, Y., *Kogyo Kagaku Zasshi* 73, 2405 (1970).
9. Bodrov, I. M., Apel'baum, L. O., and Temkin, M. I., *Kinet. Katal.* 9, 1065 (1968).
10. Ross, J. R. H., and Steel, M. C. F., *J. Chem. Soc. Faraday Trans. 1* 69, 101 (1973).
11. Sinfelt, J. H., *Catal. Rev.* 3, 175 (1969).
12. Schoubye, P., *J. Catal.* 14, 238 (1969).
13. Hougen, O. A., and Watson, K. M., "Chemical Process Principles," Part 3, p. 964. Wiley, New York, 1959.

14. Rostrup-Nielsen, J. R., *J. Catal.* 27, 343 (1972).
15. Rostrup-Nielsen, J. R., *J. Catal.* 11, 220 (1968).
16. Van Hardeveld, R., and Van Montfoort, A., *Surface Sci.* 4, 396 (1966).
17. Van Hardeveld, R., and Hartog, F., *Surface Sci.* 15, 189 (1969).
18. Van Hardeveld, R., and Hartog, F., *Proc. Int. Congr. Catal., 4th,* Moscow 1968, pap. 70; p. 295. Akademiai Kiado, Budapest, 1971.
19. Van Hardeveld, R., and Van Montfoort, A., *Surface Sci.* 17, 90 (1969).
20. Eischens, R. P., and Jacknow, J., *Proc. Int. Congr. Catal., 3rd, 1964* 1, 641 (1965).
21. King, D. A., *Surface Sci.* 9, 375 (1968).
22. Roev, L. M., Batychko, S. V., and Rusov, M. T., *Kinet. Katal.* 12, 1072 (1971).
23. Bradshaw, A. M., and Pritchard, J., *Surface Sci.* 19, 198 (1970).
24. Bradshaw, A. M., and Pritchard, J., *Surface Sci.* 17, 371 (1969).
25. Van Hardeveld, R., private communication.
26. Kjær, J., "Computer Methods in Catalytic Reactor Calculations," Vedbæk, 1972.
27. Kemball, C., *Discuss. Faraday Soc.* 41, 190 (1966).
28. Frennet, A., and Lienard, G., *Surface Sci.* 18, 80 (1969).
29. Balandin, A. A., Slovokhotova, T. A., Sholin, A. F., and Ugol'tseva, L. A., *Kinet. Katal.* 6, 115 (1965).
30. Guczi, L., Gudkov, B. S., and Tétényi, P., *J. Catal.* 24, 187 (1972).
31. Anderson, J. R., and Baker, B. G., *Proc. Roy. Soc., Ser A* 271, 402 (1963).
32. Freel, J., and Galwey, A. K., *J. Catal.* 10, 277 (1968).
33. Shephard, F. E., *J. Catal.* 14, 148 (1969).
34. Boudart, M., *AIChE J.* 18, 465 (1972).
35. Maire, G., Anderson, J. R., and Johnson, B. B., *Proc. Roy. Soc., Ser. A* 320, 227 (1970).
36. Maire, G., and Legare, P., *J. Chim. Phys. Physicochim. Biol.* 68, 1206 (1971).
37. Boudart, M., *AIChE J.* 2, 62 (1956).
38. Lička, S., thesis, Vysckáškola Chemicko-Technologická Praha, 1971.
39. Myers, C. G., and Munns, G. W., Jr., *Ind. Eng. Chem.* 50, 1727 (1958).
40. Balashova, S. A., Slovokhotova, T. A., and Balandin, A. A., *Izv. Akad. Nauk SSSR Ser. Khim.* 2, 275 (1965).
41. Yoshitomi, S., Morita, Y., and Yamamoto, K., *Bull. Jap. Petrol. Inst.* 4, 15 (1962).
42. Schnell, C. R., *J. Chem. Soc.* (B) 158 (1970).
43. Mckee, D. W., *J. Catal.* 8, 240 (1967).
44. Merkel, H., *Brennst.-Chem.* 48, 131 (1967).
45. Pour, V., *Collect. Czech. Chem. Commun.* 35, 2203 (1970).
46. Roginskii, S. S., "Adsorption und Katalyse an inhomogenen Oberflächen," p. 17. Akademie Verlag Berlin, 1958.
47. Cimino, A., Boudart, M., and Taylor, H., *J. Phys. Chem.* 58, 796 (1954).
48. Richardson, J. T., *J. Catal.* 21, 122 (1971).
49. Schwab, G.-M., Block, J., Müller, W., and Schultze, D., *Naturwissenschaften* 44, 582 (1957).
50. Szabo, Z. G., and Solymosi, F., *Actes Congr. Int. Catal.*, 2, 1627 (1961).
51. Sachtler, W. H. M., and Van der Plank, P., *Surface Sci.* 18, 62 (1969).
52. Dalla Betta R. A., and Boudart, M., *Proc. Int. Congr. Catal., 5th,* Palm Beach, FL, 1972, 2, 1329 (1973).
53. Bousquet, J. L., and Teichner, S. J., *Bull. Soc. Chim. Fr.* 10, 3687 (1972).
54. Ponec, V., and Sachtler, W. H. M., *Proc. Int. Congr. Catal., 5th,* Palm Beach, FL, 1972, 1, 645 (1973).
55. Anderson, J. R., Macdonald, R. J., and Shimoyama, Y., *J. Catal.* 20, 147 (1971).
56. Cunningham, R. E., and Gwathmey, A. T., *in* "Advances in Catalysis" (D. D. Eley, W. G. Frankenburg, V. I. Komarewsky, and P. B. Weisz, Eds.), Vol. 9, p. 25. Academic Press, New York, 1957.
57. Winterbottom, W. I., *Acta Met.* 15, 303 (1967).
58. Kingery, W. D., *J. Amer. Ceram. Soc.* 37, 42 (1954).
59. Humenik, M., Jr., and Kingery, W. D., *J. Amer. Ceram. Soc.* 37, 18 (1954).
60. Sundquist, B. E., *Acta Met.* 12, 67 (1964).
61. Armstrong, W. M., Chaklader, A. C. D., and Clarke, J. F., *J. Amer. Ceram. Soc.* 45, 115 (1962).

This Page is Inserted by IFW Indexing and Scanning Operations and is not part of the Official Record

BEST AVAILABLE IMAGES

Defective images within this document are accurate representations of the original documents submitted by the applicant.

Defects in the images include but are not limited to the items checked:

- ☐ BLACK BORDERS
- ☐ IMAGE CUT OFF AT TOP, BOTTOM OR SIDES
- ☐ FADED TEXT OR DRAWING
- ☐ BLURRED OR ILLEGIBLE TEXT OR DRAWING
- ☐ SKEWED/SLANTED IMAGES
- ☐ COLOR OR BLACK AND WHITE PHOTOGRAPHS
- ☐ GRAY SCALE DOCUMENTS
- ☑ LINES OR MARKS ON ORIGINAL DOCUMENT
- ☐ REFERENCE(S) OR EXHIBIT(S) SUBMITTED ARE POOR QUALITY
- ☐ OTHER: _____

IMAGES ARE BEST AVAILABLE COPY.
As rescanning these documents will not correct the image problems checked, please do not report these problems to the IFW Image Problem Mailbox.